

Cyclical Variational Bayes Monte Carlo for Efficient Multi-Modal Posterior Distributions Evaluation

Felipe Igea^{a*}, Alice Cicirello^{a,b}

^a Department of Engineering Science
University of Oxford
Parks Road, Oxford OX1 3PJ, UK

^b Faculty of Civil Engineering and Geosciences, Department of Engineering Structures,
Section of Mechanics and Physics of Structures (MPS)
Delft University of Technology, Stevinweg 1, Delft 2628, NL

Abstract

Statistical model updating is frequently used in engineering to calculate the uncertainty of some unknown latent parameters when a set of measurements on observable quantities is given. Variational inference is an alternative approach to sampling methods that has been developed by the machine learning community to estimate posterior approximations through an optimization approach. In this paper, the Variational Bayesian Monte Carlo (VBMC) method is investigated with the purpose of dealing with statistical model updating problems in engineering involving expensive-to-run models. This method combines the active-sampling Bayesian quadrature with a Gaussian-process based variational inference to yield a non-parametric estimation of the posterior distribution of the identified parameters involving few runs of the expensive-to-run model. VBMC can also be used for model selection as it produces an estimation of the model's evidence lower bound. In this paper, a variant of the VBMC algorithm is developed through the introduction of a cyclical annealing schedule into the algorithm.

The proposed cyclical VBMC algorithm allows to deal effectively with multi-modal posteriors by having multiple cycles of exploration and exploitation phases. Four numerical examples are used to compare the standard VBMC algorithm, the monotonic

VBMC, the cyclical VBMC and the Transitional Ensemble Markov Chain Monte Carlo (TEMCMC). Overall, it is found that the proposed cyclical VBMC approach yields accurate results with a very reduced number of model runs compared to the state of the art sampling technique TEMCMC. It is shown that for the case of low dimensional unimodal distributions, the standard VBMC might require a reduced number of model runs compared to the cyclical VBMC to obtain the same level of accuracy. However, in the presence of potential multi-modal problems, the proposed cyclical VBMC algorithm outperforms all the other approaches in terms of accuracy of the resulting posterior.

Keywords: Bayesian Inference; Variational Inference; Bayesian Quadrature; Gaussian Process; Model Updating; Cyclical Annealing;

1 Introduction

Bayesian model updating techniques are frequently used in engineering to quantify the inherent variability of some uncertain latent parameters, or to identify the unknown values of latent parameters used in physics-based models in the light of measurements of some observable quantities [1]. These statistically updated models can then be used to evaluate the behaviour of an engineering system. For example, the statistically updated model can be used for assessing the performance of a structure under various loading and environmental conditions, and/or to assess the remaining useful life of a structure [1–4]. This paper is focused on the inference of uncertain parameters encountered in engineering problems which are characterized by an expensive-to-run detailed deterministic model considered as a black-box function. The misfit between the features extracted from the measurements, and those obtained from the model are used to calculate the likelihood function that is used in the inference scheme. The goal is to present a strategy that can be implemented when only a limited number of simulation evaluations can be carried out because of computational budget and/or time constraints. This strategy enables a computationally efficient Bayesian model updating approach.

Bayesian model updating is often implemented by using sampling-based techniques [1]. However, their applicability might be limited if tight time constraints or restricted computational budget are present, as those techniques involve multiple evaluations of the expensive-to-run models used to describe the physics of the real system. Specifically, sampling techniques, including Markov Chain Monte Carlo (MCMC), show a trade-off

between computational cost and accuracy, as the convergence of the Markov Chain to the posterior distribution is improved as the chain size increases [1]. These Monte Carlo (MC) techniques introduce a bias, and the number of runs required to achieve convergence is generally unknown when starting the algorithm [1,5].

Variational inference [6] has been used by the machine learning community to estimate posterior distribution approximations employing an optimization approach for the inference problem. In simple terms, most variational inference methods propose a family of distributions where the member of the family that best approximates the posterior is chosen [6]. Compared to sampling techniques such as MCMC [7–9], the recent variational inference techniques [10–14] are more numerically scalable and may be used in a wider range of problems due to significant advances in the optimization process [6]. Nevertheless, MCMC based techniques are still the preferred method [13], as they guarantee convergence to the correct posteriors. However, the disadvantage of these techniques is their high computational cost.

The Variational Bayes Monte Carlo (VBMC) [14,15] has been recently developed to provide an efficient estimation of the model evidence and of the posterior. The method combines active-sampling Bayesian quadrature [16,17] with variational inference [6]. In a nutshell: (a) a postulated posterior is obtained using a Gaussian mixture; (b) the parameters of the Gaussian mixture are obtained using the evidence lower bound (ELBO) as the objective function to be maximised; (c) the expensive to evaluate log unnormalized posterior distribution is replaced by a statistical surrogate model constructed using a GP [18]; (d) active sampling is carried out using ‘smart’ acquisition functions applied to the GP model to perform a guided local refinement of the GP model; (e) the Bayesian quadrature [16,17] is implemented to carry out fast integrations in the variational objective. As a result, the VBMC framework [14,15] is highly efficient; (f) a warm-up process is introduced to avoid the algorithm getting initially stuck in areas of very low probability under the true posterior. During the initial phases of the warm-up, significant improvements of the ELBO are rapidly obtained; (g) the algorithm adaptively adjusts the number of components in the variational mixture, adding or removing components based on the level of improvement found on the solution. However, the application of VBMC to statistical model updating in engineering problems requires addressing the following challenges: (i) How to select the limited number of initial simulations to build the initial

GP? (ii) How to select the new samples to account for multimodality in the posterior distribution? (iii) How to quantify the accuracy of the results?

To tackle these challenges, the cyclical VBMC approach is proposed. The first (i) and second (ii) issues are tackled by introducing an artificial temperature parameter that anneals the unnormalized posterior. This parameter improves the exploration abilities and mode coverage of the algorithm, so the limitations introduced by the limited number of samples and a poor initialization are overcome. This annealing schedule enhances the exploration phase of the cycle and the discovery of regions of high probability density in multimodal posteriors, as it avoids the algorithm getting stuck in the initially found regions of high probability. For the third issue (iii), the convergence criteria developed in [14,15] are carried out at the end of each iteration of the algorithm. These metrics are functions of the expected value of the Evidence Lower Bound (ELBO), the variance of the ELBO, and the ‘Gaussianized’ symmetrized Kullback–Leibler (KL) divergence.

Ni et al [19] have recently explored the use of variational inference in combination with adaptive Gaussian process modeling for the calculation of the posterior probability density functions. In their study, two numerical applications and one experimental study were performed for the validation of the approach used for damage identification and probabilistic model updating. Their approach is shown to reduce the amount of function evaluations of the physics-based model needed to obtain reliable estimates of the probability density function of the parameters to be inferred. Compared to the work by Ni et al [19], the main differences introduced by the proposed algorithm are: (a) the use of a different acquisition function that selects new points prioritizing the areas of greater probability density compared to the acquisition function based on the absolute value of the mean divided by the standard deviation of the GP surrogate model; (b) variational whitening is performed to deal with posteriors that are highly correlated; (c) convergence criteria based on ELBO (described in (iii)) compared to the use of criteria related to the vector of variational parameters and the values of the Gaussian mixture weights; (d) the introduction of a warm-up process; (e) the adaptive adjustment of components in the variational mixture; (f) a cyclical annealing schedule to improve the exploration capabilities of the algorithm for dealing with multi-modal posteriors.

The proposed approach may benefit other engineering applications, including Bayesian Experimental Design [20–22], and optimal sensor placement frameworks based on

information theory [23,24], since it may reduce the computational cost required for the application of these approaches.

The proposed cyclical VBMC method is compared to the standard VBMC [14,15], the monotonic VBMC, and the state-of-the-art sampling approach Transitional Ensemble Markov Chain Monte Carlo (TEMCMC) [25] in several engineering examples. Both unimodal and multi-modal posteriors are used to investigate the overall performance of the proposed cyclical VBMC algorithm.

The paper is structured as follows. In section 2, the Bayesian model updating framework and variational inference are reviewed. The main building blocks on the cyclical VBMC algorithm are described in detail in section 3. The numerical results obtained are presented in section 4. The conclusions of the proposed cyclical VBMC algorithm are then discussed in section 5.

2 Bayesian Model Updating Framework

A physics-based model $PM(\mathbf{x}, \boldsymbol{\theta})$ defines the relationship between an input vector of model parameters $\{\mathbf{x}, \boldsymbol{\theta}\}$, and the output response vector \mathbf{y}_m . The vector of model parameters is described by \mathbf{x} , representing a vector with fixed properties known in advance and a vector of uncertain model parameters $\boldsymbol{\theta}$. In practice, the model response \mathbf{y}_m will be different to the true output response \mathbf{y} of the corresponding real system because of three different types of uncertainties [26]: two of them related to the model (described below), and the last one related to the measurements. The uncertainties related to the measurements are mainly caused by the sensor noise, and will lead to a discrepancy $\boldsymbol{\varepsilon}_{obs}$ between the real system response and the measurements \mathbf{y}_{obs} , so that [26]:

$$\mathbf{y}_{obs} - \mathbf{y} = \boldsymbol{\varepsilon}_{obs} \quad (1)$$

The uncertainties related to the model can be distinguished into modelling uncertainties and the uncertainties associated with the model parameters. Modelling uncertainty represents simplifications, modelling assumptions and numerical approximations that would lead to a discrepancy between the real system and the model that represents it.

These uncertainties would cause a discrepancy $\boldsymbol{\varepsilon}_m$ between the real system response and the response yielded by the model, such that [26]:

$$\mathbf{y}_m - \mathbf{y} = \boldsymbol{\varepsilon}_m \quad (2)$$

The uncertainties described in eq.(1) and eq.(2) are usually accounted for by using an additive error modelling, such that [26]:

$$\mathbf{y}_{\text{obs}} = PM(\mathbf{x}, \boldsymbol{\theta}) + \boldsymbol{\varepsilon} \quad (3)$$

where $\boldsymbol{\varepsilon}$ indicates the total prediction error caused by model uncertainties $\boldsymbol{\varepsilon}_m$ and measurement errors $\boldsymbol{\varepsilon}_{\text{obs}}$, which are usually assumed to be independent and identically distributed [4].

The main task in the Bayesian model updating framework [3] is then to update knowledge on the uncertain model parameters $\boldsymbol{\theta}$ of the physics-based model by using measurements \mathbf{y}_{obs} taken on the real system.

2.1 From prior knowledge and data to a posterior distribution

The Bayesian model updating strategy enables the combination of a physics-based model that includes uncertain parameters $\boldsymbol{\theta}$ which cannot be directly observed (also known as latent variables), described by probability density functions, the so-called prior distribution, with new information obtained from measurements of some observable quantities \mathbf{y}_{obs} [2,3]. This new information is encoded in the so-called likelihood distribution. This approach results into an updated physics-based model with parameters described as probability density functions, the so-called posterior distributions. This statistical updated model, that is more representative of the real system, can then be used to investigate the behaviour of the system under different loading conditions in order to predict its performance with respect to safety, quality, design or cost constraints [1–4].

In particular, a prior probability density function $p(\boldsymbol{\theta})$ that reflects the prior knowledge of the uncertain parameters $\boldsymbol{\theta}$ before any measurements on some observable variables \mathbf{y} are taken, is assigned to the parameters. Then a likelihood function $p(\mathbf{y}_{\text{obs}} | \boldsymbol{\theta})$ should be chosen to reflect the level of acceptability of the physics-based model, given a set of uncertain parameters $\boldsymbol{\theta}$ to describe the measurements obtained. To do so, the likelihood function $p(\mathbf{y}_{\text{obs}} | \boldsymbol{\theta})$ is constructed by using features extracted (e.g., natural frequencies) from the response obtained with the physics-based model, and the corresponding ones extracted from some measurements. These measurements can be expressed in different

forms such as time history, modal properties, etc. The posterior probability density functions $p(\boldsymbol{\theta} | \mathbf{y}_{\text{obs}})$ of the uncertain parameters of the physics-based model can then be calculated using [2,3]:

$$p(\boldsymbol{\theta} | \mathbf{y}_{\text{obs}}) = \frac{p(\boldsymbol{\theta})p(\mathbf{y}_{\text{obs}} | \boldsymbol{\theta})}{p(\mathbf{y}_{\text{obs}})} \quad (4)$$

where $p(\mathbf{y}_{\text{obs}})$ is defined as the evidence, and it serves as a normalization constant for the posterior probability density functions. The posterior $p(\boldsymbol{\theta} | \mathbf{y}_{\text{obs}})$ can be computed analytically if the prior and likelihood distributions are part of the conjugate family. However, this is not necessarily always the case, and therefore, numerical integration may be necessary.

As the evidence term in Bayesian Inference is a numerical constant, and it is independent of the uncertain parameters $\boldsymbol{\theta}$ [1], sampling techniques (e.g., MCMC) [27–29] can be used to obtain samples from the posterior distribution using the following proportional relationship:

$$p(\boldsymbol{\theta} | \mathbf{y}_{\text{obs}}) \propto p(\boldsymbol{\theta})p(\mathbf{y}_{\text{obs}} | \boldsymbol{\theta}) \quad (5)$$

However, the applicability of sampling methods becomes more limited as engineering problems grow in complexity, requiring more intricate models to describe their physical behaviour [14,15]. Those high-dimensional and multi-modal engineering problems require the evaluation of multiple expensive likelihoods for model parameter inference [14,15]. Variational inference takes an alternative approach by minimising the KL divergence between the best member of the postulated family and the posterior density, and therefore bypassing the calculation of the evidence term [6]. The posterior distribution is then obtained by transforming the statistical inference problem into an optimization problem, as reviewed in what follows.

2.2 Review of Variational Inference

In variational inference [6] a family of densities Q is postulated as an approximation to the posterior density $p(\boldsymbol{\theta} | \mathbf{y}_{\text{obs}})$, where the optimization scheme chooses the member of the family $q(\boldsymbol{\theta})$ that is ‘closest’ to the posterior density. The choice of members of the family is performed in such a manner that it is flexible enough to capture the posterior density and simple enough to be optimized [6]. In variational inference, ‘over-fitting’ the

posterior density by using highly flexible distributions is not a problem, as the highly flexible distributions allow better approximations of the true posterior distribution [30].

Variational inference chooses the optimal member $q(\boldsymbol{\theta})$ of the family \mathcal{Q} by solving the following optimization problem [6]:

$$q^*(\boldsymbol{\theta}) = \arg \min_{q(\boldsymbol{\theta}) \in \mathcal{Q}} KL(q(\boldsymbol{\theta}) \| p(\boldsymbol{\theta} | \mathbf{y}_{\text{obs}})) \quad (6)$$

Where KL is the Kullback-Leibler divergence (also called relative entropy), defined as:

$$KL(q(\boldsymbol{\theta}) \| p(\boldsymbol{\theta} | \mathbf{y}_{\text{obs}})) \equiv \int_{\mathbf{R}^d} q(\boldsymbol{\theta}) \log \left(\frac{q(\boldsymbol{\theta})}{p(\boldsymbol{\theta} | \mathbf{y}_{\text{obs}})} \right) d\boldsymbol{\theta} \quad (7)$$

and \mathbf{R}^d is given by the real coordinate space of dimension d .

The KL divergence is a measure of how different a distribution is from a second reference distribution. The KL divergence is always non-negative $KL(q(\boldsymbol{\theta}) \| p(\boldsymbol{\theta} | \mathbf{y}_{\text{obs}})) \geq 0$ and is non-symmetric (i.e., $KL(q(\boldsymbol{\theta}) \| p(\boldsymbol{\theta} | \mathbf{y}_{\text{obs}})) \neq KL(p(\boldsymbol{\theta} | \mathbf{y}_{\text{obs}}) \| q(\boldsymbol{\theta}))$). When the distributions are the same i.e., $q(\boldsymbol{\theta}) \equiv p(\boldsymbol{\theta} | \mathbf{y}_{\text{obs}})$, the KL divergence is minimised and therefore returns a value of zero [31].

However, the calculation of the optimal member $q(\boldsymbol{\theta})$ of the family of densities \mathcal{Q} that minimises the $KL(q(\boldsymbol{\theta}) \| p(\boldsymbol{\theta} | \mathbf{y}_{\text{obs}}))$ in eq.(6) cannot be analytically computed, as the evidence term $p(\mathbf{y}_{\text{obs}})$ should be known, as shown below [6]:

$$KL(q(\boldsymbol{\theta}) \| p(\boldsymbol{\theta} | \mathbf{y}_{\text{obs}})) = E_q [\log q(\boldsymbol{\theta})] - E_q [\log p(\boldsymbol{\theta} | \mathbf{y}_{\text{obs}})] \quad (8)$$

$$KL(q(\boldsymbol{\theta}) \| p(\boldsymbol{\theta} | \mathbf{y}_{\text{obs}})) = E_q [\log q(\boldsymbol{\theta})] - E_q [\log p(\boldsymbol{\theta}, \mathbf{y}_{\text{obs}})] + \log p(\mathbf{y}_{\text{obs}}) \quad (9)$$

where E_q indicates the expectation with respect to $q(\boldsymbol{\theta})$.

As the KL divergence between the posterior approximation $q(\boldsymbol{\theta})$ and the posterior $p(\boldsymbol{\theta} | \mathbf{y}_{\text{obs}})$ cannot be directly computed, the objective function is changed to the evidence lower bound (ELBO), which is equivalent to the negative KL divergence between the prior $p(\boldsymbol{\theta})$ and posterior approximation $q(\boldsymbol{\theta})$, plus a constant [6]:

$$ELBO(q) = E_q [\log p(\boldsymbol{\theta}, \mathbf{y}_{\text{obs}})] - E_q [\log q(\boldsymbol{\theta})] = E_q [\log p(\mathbf{y}_{\text{obs}} | \boldsymbol{\theta})] - KL(q(\boldsymbol{\theta}) \| p(\boldsymbol{\theta})) \quad (10)$$

Therefore, maximizing the ELBO objective function in eq.(10), is equivalent to the

minimization of the KL divergence between the posterior approximation $q(\boldsymbol{\theta})$ and the posterior $p(\boldsymbol{\theta} | \mathbf{y}_{\text{obs}})$ [14]:

$$\arg \max_{q(\boldsymbol{\theta}) \in \mathcal{Q}} ELBO(q(\boldsymbol{\theta})) \equiv \arg \min_{q(\boldsymbol{\theta}) \in \mathcal{Q}} KL(q(\boldsymbol{\theta}) \| p(\boldsymbol{\theta} | \mathbf{y}_{\text{obs}})) \quad (11)$$

In engineering problems, due to the complexity of the physics-based models, the term $E_q [\log p(\boldsymbol{\theta} | \mathbf{y}_{\text{obs}})]$ does not have a convenient form which allows for a closed-form solution of eq.(10). Factorised posteriors are usually chosen (e.g., mean-field variational inference [32,33]) where the choice of the family \mathcal{Q} and the parametric form of the

member that best approximates the posterior $q(\boldsymbol{\theta})$, is given by $q(\boldsymbol{\theta}) = \prod_{i=1}^d q_i(\theta_i)$, where

d is the number of parameters to be inferred. These factorised posteriors simplify the optimization procedure in eq.(11) at the cost of the accuracy of the approximation of the posterior $p(\boldsymbol{\theta} | \mathbf{y}_{\text{obs}})$. Nonetheless, in typical engineering applications, the likelihood can only be evaluated by running an expensive black-box model that increases the computational cost, to the point of being unfeasible, even when using the mean-field algorithm [6].

In computer science, several approaches [11–15,34,35] have been developed to circumvent the need of an analytical expression of the ELBO equation, and to reduce the number of evaluations of the physics-based model to be carried out. One of these approaches is the Variational Bayesian Monte Carlo (VBMC) [14,15]. In this paper, a variant of the approach called cyclical VBMC is proposed for addressing the statistical updating problems in engineering where multi-modal posteriors are expected.

3 Cyclical Variational Bayesian Monte Carlo framework

The cyclical VBMC approach is based on the VBMC algorithm, it has been developed to deal with multi-modal posteriors in an efficient way by introducing an artificial temperature parameter that anneals the unnormalized posterior. The proposed method overcomes the drawbacks of limited function evaluations and a poor initialization of the VBMC algorithm by introducing the cyclical schedule that improves the exploration abilities and mode coverage of the algorithm.

Given an expensive-to-evaluate computational model of an engineering system, for which prior information on the unknown latent parameters and measurements obtained from the

engineering system are available, the proposed approach aims at minimising the number of function evaluations compared to state of the art Bayesian sampling approaches, while obtaining an accurate description of the posterior. The approach consists of two main parts: the initialization of the algorithm and the procedure used to update the parameters in the posterior variational distribution. These two main parts are shown in Fig. 1 and Fig. 2 respectively.

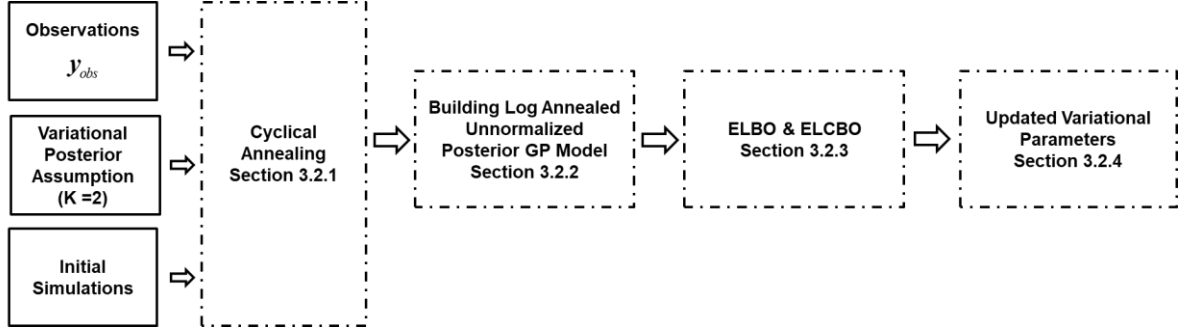


Fig. 1. Initialization Blocks of Cyclical VBMC Algorithm.

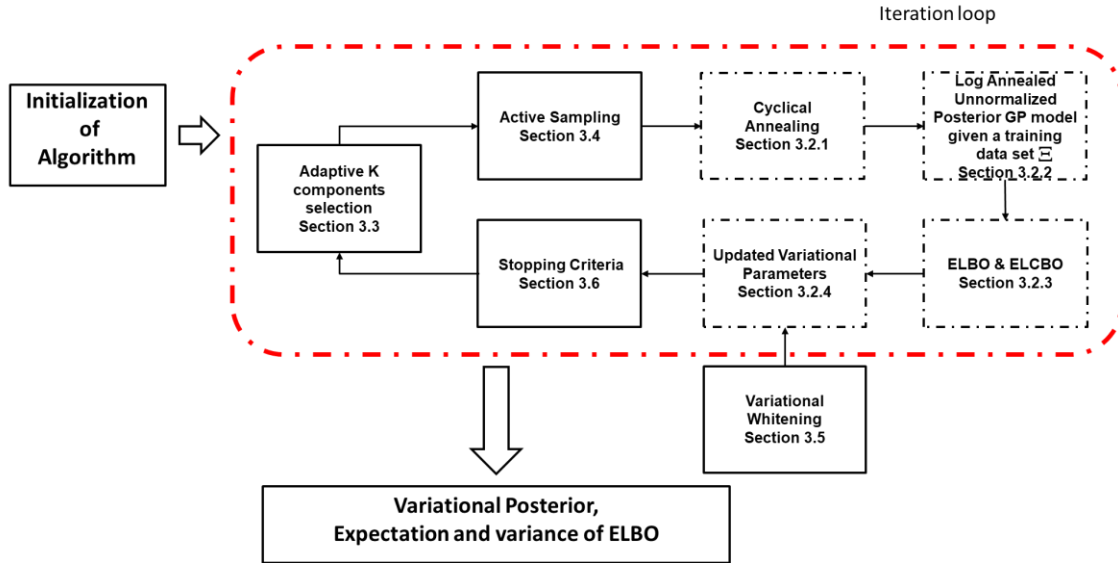


Fig. 2. Cyclical VBMC Algorithm Blocks.

The initialization of the algorithm shown in Fig. 1 begins with assuming a variational posterior that is flexible, and able to capture complex smooth posteriors. This is done by using a Gaussian mixture as the postulated posterior. Then, an initial set of parameters that is given as input to the physics-based simulation is chosen, and its output is calculated. Given an assumed prior and likelihood function, the logarithm of the unnormalized posterior is calculated. Cyclical annealing is also introduced by replacing the log unnormalized posterior values with the annealed log unnormalized posterior

values. A Gaussian Process (GP) regression model using as training points the logarithm of the annealed unnormalized posterior values is employed to build a probabilistic surrogate of the logarithm of the annealed unnormalized posterior. Using Bayesian quadrature [16,17], the GP can then be used to calculate the ELBO and evidence lower confidence bound (ELCBO) values. Finally, the updated variational parameters are obtained.

The second part of the algorithm shown in Fig. 2, consists of a total of T iterations, and it starts with active sampling to select samples for the physics-based model that are run at locations that maximize an acquisition function. The acquisition function is chosen in such a manner that sampling is encouraged at high probability regions of the log unnormalized posterior. Cyclical annealing is introduced into the algorithm by replacing the log unnormalized posterior with the annealed log unnormalized posterior. A prescribed number of cycles and total iterations is set to produce both, an exploration phase and an exploitation phase. The GP regression model is built and the GP's hyperparameters are automatically set by using the maximum-a-posteriori estimates. This is done employing initially slice sampling [36], and subsequently gradient based optimization as recommended to improve computational efficiency in [14,15]. Bayesian Quadrature [16,17] is used to calculate the value of the ELBO. The ELCBO is also calculated, and employed to evaluate the variational approximation's improvement and also as a convergence diagnostic. For each iteration, the stochastic gradient ascent is used to update the parameters of the variational posterior. Variational whitening is also performed every few iterations to deal with highly correlated posteriors. Once the stopping criteria have been fulfilled, the method returns the variational approximation of the posterior, and the expectation and variance of the ELBO.

More details about the approach setup, core building blocks (dashed blocks of Fig. 1 and Fig. 2), adaptive K components selection, active sampling, variational whitening and stopping criteria are given in the following subsections.

3.1 Approach setup

Given a set of observation \mathbf{y}_{obs} and a model $PM(\mathbf{x}, \boldsymbol{\theta})$ the setup used in the cyclical VBMC algorithm is described in the following subsections.

3.1.1 Variational approximation of the posterior $q(\theta)$

The selection of the variational posterior $q(\theta)$ is flexible [12], and it should be made with the intent to capture the complex posteriors $p(\theta | \mathbf{y}_{obs})$ that can be encountered in engineering applications.

Without loss of generality, the variational posterior $q(\theta)$ can be expressed with a non-parametric approximation that is provided by a Gaussian mixture with K components [14,15]:

$$q(\theta) = \sum_{k=1}^K w_k \mathcal{N}(\theta; \mu_k, \gamma_k^2 \Sigma) \quad (12)$$

where the mixture weight, mean and scale factor are respectively given by w_k, μ_k, γ_k^2 , and Σ is the covariance matrix:

$$\Sigma = \text{diag} \left[\lambda^{(1)^2}, \dots, \lambda^{(d)^2} \right] \quad (13)$$

The variational posterior is parameterized in terms of the vector of parameters $\phi \equiv (w_1, \dots, w_K, \mu_1, \dots, \mu_K, \gamma_1, \dots, \gamma_K, \lambda)$. As a result, the number of parameters to optimise in the variational posterior $q_\phi(\theta)$ is given by $d + (d + 2)K$, which is the length of the vector ϕ .

3.1.2 Selection of Initial Physics-Based Simulations

Given the uncertain parameters θ , the initial step requires samples to be generated. If available, the plausible lower bound (PLB) and plausible upper bound (PUB) which limit the region of the parameter space of high posterior probability mass should be specified. A set of points (as a rule-of-thumb a total of 10 points) situated in the plausible box would be uniformly distributed at random [14,15].

It might occur that the PLB and PUB are not known. In that case, a set of initial points can be chosen using different sampling methods such as Latin Hypercube Sampling (LHS) [37]. LHS is used in the numerical examples shown in section 4.

The initial points $\Theta_0 = [\theta_1, \dots, \theta_{n_{init}}]$ are used as inputs for the physics-based model to obtain the output response, where n_{init} is the total number of initial points. The output response can be used to construct features that are then used to evaluate the likelihood

values given an assumed likelihood function. The likelihood function reflects the level of agreement between the features obtained by the mathematical model and the measurements. Then, the unnormalized posterior of the initial points can be calculated to build the GP of the annealed logarithm of the unnormalized posterior as described in subsection 3.2.2.

3.2 Core building blocks

3.2.1 Cyclical Annealing

The annealing process is used to flatten the objective function (the ELBO), and to reduce the chance of the algorithm getting stuck in some local optima of the parameters of the variational posterior. The annealing process produces a deterministic deformation of the objective function [38], by means of a temperature parameter [25]:

$$p(\boldsymbol{\theta} | \mathbf{y}_{\text{obs}})^{\frac{1}{temp}} \propto [p(\boldsymbol{\theta})p(\mathbf{y}_{\text{obs}} | \boldsymbol{\theta})]^{\frac{1}{temp}} \quad (14)$$

A fixed temperature implies that the true objective is optimized at a constant schedule, as implemented in the standard VBMC algorithm. Monotonic annealing schedules, in which the temperature is progressively reduced, are the most frequently used. The temperature decreases until the algorithm reaches the true posterior [39].

The cyclical annealing schedule [39–42] has been used to deal with complex posteriors in the machine learning field. Here, it is introduced to yield a better representation of the posterior through the introduction of an exploration phase with improved target guidance. Specifically, two phases, exploration and exploitation may be found if the temperature is decreased from its maximum to its minimum within each cycle. These phases are cyclically repeated for a prescribed number of times to improve convergence. This enables the algorithm to explore areas of high probability density that may otherwise have not been found. Specifically, during the exploration phase, “paths” would start forming in regions where sampling would take place, producing a high coverage of the support of the target distribution. During the exploitation phase, sampling takes place at regions of high probability density. Therefore, the cyclical schedule gradually improves convergence by reopening paths, and by leveraging on the previous cycles as warm re-starts.

The temperature parameter is the inverse of the parameter β_i :

$$temp = 1 / \beta_t \quad (15)$$

The parameter β_t is defined in the interval $[0,1]$, and it is calculated for each iteration step in the cyclical VBMCM algorithm. According to [39], the β_t can be expressed as:

$$\beta_t = \begin{cases} \frac{\tau}{S}, & \tau \leq S \\ 1, & \tau > S \end{cases} \quad (16)$$

where:

$$\tau = \frac{\text{mod}(t-1, [S/M])}{S/M} \quad (17)$$

and $t = 1:1:T$ is the iteration number, T is the number of total iterations for the annealing schedule, M is the number of cycles, and S is a control parameter. The exceptional case of $\beta_t = 0$ is circumvented by defining $temp$ as an interval variable $temp \in [1,50]$. The control parameter S is set to 0.5 as described in [39].

As a rule-of-thumb, if the user has a maximum number of simulations available N_{sim} (e.g., 1000), 20% of these simulations (200) will be allocated for carrying out the cyclical annealing schedule. Therefore, the total number of iterations for the cyclical annealing is obtained by considering the total number of simulations assigned per iteration (for example, 5 simulations per iteration would lead to a total of $T = 40$ iterations of the cyclical annealing schedule). The choice of the number of cycles M depends on the trade-off between exploration and exploitation that the user wants to investigate. For example, if $M = 5$, it would mean that 8 iterations form 1 cycle, in which the temperature (eq.(15)) decreases from its maximum to 1. Once the number of total number of iterations for the cyclical annealing schedule has been reached, the temperature is set to 1.

To introduce the cyclical annealing schedule into the algorithm, the log unnormalized posterior $\log p(\boldsymbol{\theta}, \mathbf{y}_{obs})$ is replaced with the annealed log unnormalized posterior $\log p_{annealed}(\boldsymbol{\theta}, \mathbf{y}_{obs})$, that is defined as:

$$\log p_{annealed}(\boldsymbol{\theta}, \mathbf{y}_{obs}) = \frac{1}{temp} \log p(\boldsymbol{\theta}, \mathbf{y}_{obs}) \quad (18)$$

3.2.2 Gaussian process (GP) of the annealed logarithm unnormalized posterior

For the proposed cyclical VBMC, cyclical tempering is introduced into the algorithm, by simply replacing the log unnormalized posterior $f \equiv \log p(\boldsymbol{\theta}, \mathbf{y}_{\text{obs}})$ with the annealed log unnormalized posterior $f \equiv \log p_{\text{annealed}}(\boldsymbol{\theta}, \mathbf{y}_{\text{obs}})$.

The annealed log unnormalized posterior $f \equiv \log p_{\text{annealed}}(\boldsymbol{\theta}, \mathbf{y}_{\text{obs}})$, is approximated using a GP regression model [18]:

$$f \sim GP(m_{gp}(\boldsymbol{\theta}), k_{gp}(\boldsymbol{\theta}, \boldsymbol{\theta}')) \quad (19)$$

where $m_{gp}(\boldsymbol{\theta})$ is the mean function, and a covariance matrix is defined in terms of a kernel function $k_{gp}(\boldsymbol{\theta}, \boldsymbol{\theta}')$. The typical choice when little is known about the function to be approximated [18] is to use the squared exponential kernel that is expressed as:

$$k_{gp}(\boldsymbol{\theta}, \boldsymbol{\theta}') = \sigma_f^2 \Lambda \exp\left(-\frac{1}{2}(\boldsymbol{\theta} - \boldsymbol{\theta}')^T \Sigma_l^{-1} (\boldsymbol{\theta} - \boldsymbol{\theta}')\right) \quad (20)$$

Where σ_f is the output length scale, and:

$$\Lambda \equiv (2\pi)^{\frac{d}{2}} \prod_{i=1}^d l^{(i)} \quad (21)$$

is the normalization of the Gaussian, with d representing the number of unknown parameters to be inferred (i.e., length of the vector of uncertain parameters $\boldsymbol{\theta}$), \mathbf{l} is the vector of input length scales, the superscript $^{(i)}$ refers to the i -th dimension and Σ_l is a diagonal covariance matrix:

$$\Sigma_l = \text{diag}(l^{(1)^2}, \dots, l^{(d)^2}) \quad (22)$$

The likelihood is assumed to be Gaussian with an observation noise $\sigma_{\text{obs}} > 0$ (to obtain numerical stability [43]), and the shape of the mean function is assumed to be given by [14,15]:

$$m_{gp}(\boldsymbol{\theta}) = m_0 - \frac{1}{2} \sum_{i=1}^d \frac{(\boldsymbol{\theta}^{(i)} - \boldsymbol{\theta}_{\text{max}}^{(i)})^2}{r^{(i)^2}} \quad (23)$$

Where m_0 is the mean's maximum value, $\boldsymbol{\theta}_{\text{max}}$ is the location of the mean's maximum value, and \mathbf{r} is the length scales' vector [14,15].

The hyperparameters that define the GP are collected in a vector $\boldsymbol{\psi} = [\boldsymbol{l}, \sigma_f, \sigma_{obs}, m_0, \boldsymbol{\theta}_m, \boldsymbol{r}]$, of dimensions $3d+3$. These hyperparameters $\boldsymbol{\psi}$, are themselves defined in terms of a uniform distribution or a truncated Student's t distribution with mean μ , standard deviation σ , and $\nu = 3$ degrees of freedom. Some of these GP hyperparameters $[\boldsymbol{l}, \sigma_f, \sigma_{obs}, \boldsymbol{r}]$ are defined in the log space. The same distributions used in references [15] have been directly implemented and are given in Table 1.

Table 1

Table of hyperparameters' prior.

Hyperparameter	Description	Prior mean	Prior scale
$\log l^{(i)}$	Input length scale (i-th dimension)	$\log \left[\sqrt{\frac{d}{6}} L^{(i)} \right]$	$\log \sqrt{10^3}$
$\log \sigma_f$	Output scale	Uniform	-
$\log \bar{\sigma}_{obs}$	Base observation noise	$\log \sqrt{10^{-5}}$	0.5
m_0	Mean function maximum	Uniform	-
$\theta_{\max}^{(i)}$	Mean function location (i-th dimension)	Uniform	-
$\log r^{(i)}$	Mean function scale (i-th dimension)	Uniform	-

$L^{(i)}$ is defined by:

$$L^{(i)} = PUB^{(i)} - PLB^{(i)} \quad (24)$$

Where the PLB and PUB limit the region of the parameter space of high posterior probability mass.

The maximum-a-posteriori of the hyperparameters is first calculated using slice sampling, and the estimation is subsequently switched to a gradient based optimization approach when the variability of the expected log unnormalized posterior is below a threshold [14,15].

By conditioning, the resulting GP predictive posterior mean function $\bar{f}_{\Xi}(\boldsymbol{\theta})$ and posterior covariance function $C_{\Xi}(\boldsymbol{\theta}, \boldsymbol{\theta}')$ for a training data set $\Xi = \{\boldsymbol{\theta}, \mathbf{h}, \sigma_{obs}\}$ (for N training inputs $\boldsymbol{\theta} = [\boldsymbol{\theta}_1, \dots, \boldsymbol{\theta}_N]$, and N observations $\mathbf{h} = f(\boldsymbol{\theta})$ with observation noise $\sigma_{obs} > 0$) is given in closed-form [18] as:

$$\bar{f}_{\Xi}(\boldsymbol{\theta}) \equiv \mathbb{E}[f(\boldsymbol{\theta}) | \Xi, \boldsymbol{\psi}] = k(\boldsymbol{\theta}, \boldsymbol{\theta}) [k(\boldsymbol{\theta}, \boldsymbol{\theta}) + \Sigma_{obs}(\boldsymbol{\theta})]^{-1} (\mathbf{h} - m(\boldsymbol{\theta})) + m(\boldsymbol{\theta}) \quad (25)$$

$$C_{\Xi}(\boldsymbol{\theta}, \boldsymbol{\theta}') \equiv Cov[f(\boldsymbol{\theta}), f(\boldsymbol{\theta}') | \Xi, \boldsymbol{\psi}] = k(\boldsymbol{\theta}, \boldsymbol{\theta}') - k(\boldsymbol{\theta}, \boldsymbol{\theta}) [k(\boldsymbol{\theta}, \boldsymbol{\theta}) + \Sigma_{obs}(\boldsymbol{\theta})]^{-1} k(\boldsymbol{\theta}, \boldsymbol{\theta}') \quad (26)$$

The observation noise matrix has the following form:

$$\Sigma_{obs} = diag(\sigma_{obs}^2(\boldsymbol{\theta}_1), \dots, \sigma_{obs}^2(\boldsymbol{\theta}_N)) \quad (27)$$

As the annealed log unnormalized posterior $\log p_{annealed}(\boldsymbol{\theta}, \mathbf{y}_{obs})$ is approximated using a GP model, an analytical computation of the integral involved in the ELBO and ELCBO equation can be derived using Bayesian Quadrature [16,17], as described in what follows.

3.2.3 The Evidence Lower Bound (ELBO) and Evidence Confidence Lower Bound (ELCBO)

The ELBO can now be expressed as [14]:

$$ELBO(\phi, f) = \mathbb{E}_q[\log p(\boldsymbol{\theta}, \mathbf{y}_{obs})] - \mathbb{E}_q[\log q(\boldsymbol{\theta})] = \mathbb{E}_{f|\Xi}[\mathbb{E}_{\phi}[f]] + \mathcal{H}[q(\boldsymbol{\theta})] \quad (28)$$

Where $\mathcal{H}[q(\boldsymbol{\theta})]$ is the entropy of the variational posterior [14]. The integrals in eq.(28) can be analytically computed [14,15] with the Bayesian MC statistical method also known as Bayesian quadrature [16,17], so that [44]:

$$\mathbb{E}_{f|\Xi}[Z] = \int \bar{f}_{\Xi}(\boldsymbol{\theta}) \pi(\boldsymbol{\theta}) d\boldsymbol{\theta} \quad (29)$$

$$\mathbb{V}_{f|\Xi}[Z] = \int \int C_{\Xi}(\boldsymbol{\theta}, \boldsymbol{\theta}') \pi(\boldsymbol{\theta}) \pi(\boldsymbol{\theta}') d\boldsymbol{\theta} d\boldsymbol{\theta}' \quad (30)$$

where:

$$Z = \int_{\mathbb{R}^d} g(\boldsymbol{\theta}) \pi(\boldsymbol{\theta}) d\boldsymbol{\theta} \quad (31)$$

In the proposed cyclical VBMC algorithm the function $g(\boldsymbol{\theta})$ is given by the annealed log unnormalized posterior $\log f(\boldsymbol{\theta}) \equiv \log p_{annealed}(\boldsymbol{\theta}, \mathbf{y}_{obs})$ and $\pi(\boldsymbol{\theta})$ is the variational approximation to the posterior $q(\boldsymbol{\theta})$ [11,13].

The variational approximation's $\mathcal{H}[q(\boldsymbol{\theta})]$ entropy is calculated using Monte Carlo sampling, and the gradient is propagated using a reparameterization trick [35,45], which allows stochastic gradient ascent [46] to be used to optimize the ELBO equation.

The evidence lower confidence bound (ELCBO) is [14]:

$$ELCBO(\boldsymbol{\phi}, f) = \mathbb{E}_{f|\Xi} [\mathbb{E}_{\boldsymbol{\phi}} [f]] + \mathcal{H}[q(\boldsymbol{\theta})] - \beta_{LCB} \sqrt{\mathbb{V}_{f|\Xi} [\mathbb{E}_{\boldsymbol{\phi}} [f]]} \quad (32)$$

where the term β_{LCB} represents a risk-sensitivity term.

The ELCBO is the probabilistic lower bound of the ELBO, and it can be used to judge the variational approximation's improvement. As $\mathbb{V}_{f|\Xi} [\mathbb{E}_{\boldsymbol{\phi}} [f]]$ in eq.(32) decreases, the ELCBO value will converge to the ELBO value [14].

The two first terms of the ELCBO equation are estimated as described before. The risk sensitivity term [14] is usually set to $\beta_{LCB} = 3$.

3.2.4 Update of Variational Parameters

The variational posterior is parameterized in terms of the variational parameters in the vector $\boldsymbol{\phi}$. These variational parameters are updated by solving an optimization problem [14,15]:

$$\hat{\boldsymbol{\phi}} = \arg \max_{\boldsymbol{\phi}} \{ELBO(\boldsymbol{\phi}, f)\} \quad (33)$$

This optimization is carried out using a stochastic gradient descent algorithm based on a variant of Adam [47] to obtain the updated variational posterior.

3.3 Adaptive K components selection

A warm-up stage is used in the initial iterations of the algorithm. In this phase, the variational posterior is specified in terms of a $K=2$ Gaussian mixture with $w_1 \equiv w_2 = 0.5$. The warm-up phase finishes when the improvement of the ELCBO for three consecutive iterations is smaller than 1, this implies that the variational solution is stabilizing.

An adequate number of components K should be used to capture the true posterior [12]. The number of components in the Gaussian mixture used for the approximation is adaptively chosen as described in [14]. For this purpose, a component can be added to or removed from the Gaussian mixture. A component is added to the Gaussian mixture after the ELCBO of the current iteration is greater than the ELCBO found in the last four iterations. This is done as long as during the last iteration no mixture component was removed, an additional condition can also be set to speed up the approximation as explained in [14,15]. A component of the Gaussian mixture can also be randomly removed from the variational solution, if it simultaneously occurs that the mixture weight is smaller than 0.01, and the difference between the ELCBO of the variational solution in this iteration, and the ELCBO of the variational solution after removal of that component, is smaller than 0.01. More information can be found in [14,15].

3.4 Active Sampling

Active sampling is employed to select a number of prescribed samples within each iteration at locations which maximize an acquisition function.

These samples are the input parameters for which the physics-based model is evaluated. The acquisition function a_{pro} , is chosen in such a manner that sampling is encouraged at high probability regions of the log unnormalized posterior [14,15]:

$$a_{pro}(\boldsymbol{\theta}) = s_{\Xi}^2(\boldsymbol{\theta}) \exp(f_{\Xi}(\boldsymbol{\theta})) q_{\phi}(\boldsymbol{\theta}) \quad (34)$$

where $s_{\Xi}^2(\boldsymbol{\theta})$ is the variance of the GP posterior, $\exp(f_{\Xi}(\boldsymbol{\theta}))$ is the exponentiated GP posterior mean for a given training set Ξ , and $q_{\phi}(\boldsymbol{\theta})$ is the variational approximation of the posterior at $\boldsymbol{\theta}$.

Therefore, this acquisition function favours mostly exploitation of the knowledge obtained in the previous iterations. To add an exploration phase, cyclical annealing is also introduced. This enables the algorithm to explore areas of high probability density that may otherwise have not been found. As shown in the first and second numerical example, cyclical annealing allows sampling of multi-modal regions as an exploration phase occurs in the initial iterations of each annealing cycle. Due to the exploitation nature of the acquisition function, the last iterations of each annealing cycle start sampling at the already found modes.

3.5 Variational whitening

To deal with highly correlated posterior distributions, variational whitening is introduced in the cyclical VPMC algorithm. This is carried out using a linear transformation of the inference space to a new space where the covariance matrix results in a unit diagonal matrix [15]. The transformation matrix w (rotation and scaling) is obtained using singular value decomposition (SVD) of the covariance matrix of the variational posterior $q(\theta)$. Variational whitening occurs after the reliability index $\rho(t)$ described in the next subsection is lower and or equal to 3. It is applied in increasingly spaced intervals within iterations as illustrated in [15].

3.6 Stopping Criteria

To determine the number of required iterations, the algorithm uses a reliability index $\rho(t) \geq 0$, that suggests the stability of the variational solution. The algorithm is finished if the value $\rho(t) \leq 1$ is found at the end of $n_{stable} = 8$ consecutive iterations, where a maximum of one intermediate iteration may be unstable, or if a predetermined number of iterations n_{max} is reached.

The value at iteration t of the reliability index is calculated as the average of the three reliability features $\rho_j(t)$ for $j=1,2,3$:

$$\rho(t) = \frac{\rho_1(t) + \rho_2(t) + \rho_3(t)}{3} \quad (35)$$

The value of the reliability index $\rho_1(t)$ is calculated as a function of the KL divergence between the previous and the current variational posterior. The reliability index $\rho_2(t)$ is a function of the change of ELBO between two consecutive iterations and $\rho_3(t)$ is a function of the estimation of the variance of the ELBO. These indices give an overall measure of how the variational posterior is converging throughout the iterations and are defined as [14,15]:

$$\rho_1(t) = \frac{|E[ELBO(t)] - E[ELBO(t-1)]|}{\Delta_{SD}} \quad (36)$$

$$\rho_2(t) = \frac{\sqrt{V[ELBO(t)]}}{\Delta_{SD}} \quad (37)$$

$$\rho_3(t) = \frac{KL(q_t \| q_{t-1}) + KL(q_{t-1} \| q_t)}{2\Delta_{KL}} \quad (38)$$

The parameters Δ_{KL} and Δ_{SD} should be chosen in such a manner that the values of the individual reliability features meet the inequality $\rho_j \lesssim 1$, where $j = 1, 2, 3$, for the values of $\rho(t)$ considered representative of good solutions. In the cyclical VBMC algorithm, the values of Δ_{SD} and Δ_{KL} are respectively set at 0.1 and $0.01\sqrt{d}$.

3.7 Steps of the approach

The proposed approach can be summarised in the following steps:

1. Initialization of Algorithm (Fig. 1):
 - a. Initial training set for physics-based simulation is run.
 - b. Cyclical Annealing is introduced (eq.(18)).
 - c. Logarithm of (annealed) unnormalized posterior of the initial set is calculated.
 - d. GP surrogate model of the (annealed) logarithm unnormalized is built using the initial training set values calculated in 1.b.
 - e. ELBO and ELCBO are calculated (eq.(28) and eq.(32)).
2. Second part of the algorithm (Fig. 2):
 - a. Selection of new samples using an acquisition function (eq.(34)), these are used to actively update the GP surrogate model.
 - b. Cyclical Annealing is introduced (eq.(18)).
 - c. The GP surrogate model of the (annealed) logarithm unnormalized posterior is built.
 - d. Calculation of ELBO and ELCBO value (eq.(28)) and eq.(32)).
 - e. Update the variational parameters (variational whitening may also be applied at this step).
 - f. Check if stopping criteria have been met, if not repeat from step 2.a.

Where the main outputs of the algorithm are the variational posterior, the expected value of the ELBO, and the variance of the ELBO.

4 Numerical Analysis

This numerical analysis section has the purpose of comparing the proposed cyclical VBMC algorithm with the standard VBMC algorithm, the monotonic VBMC algorithm and the Transitional Ensemble Markov Chain Monte Carlo (TEMCMC) sampling

algorithm. The functions `plotmatrix` and `ksdensity` from MATLAB [48] were used to plot the posterior distributions obtained with the TEMCMC algorithm.

The number of function evaluations, the number of iterations used to achieve convergence, and the number of modes found, are used to compare the performance of the algorithms on the multi-modal examples. On the unimodal examples, for the same purpose, the samples mean, coefficient of variation, number of function evaluations and number of iterations are used. For all the VBMC implementations, 300,000 samples of the variational posterior are taken to compute the sample mean and sample coefficient of variation.

Ten initial samples are picked using LHS [37] for all the numerical examples that use a form of the VBMC algorithm, and for every iteration that occurs within the algorithm, five samples are chosen using the acquisition function, and are evaluated. The samples chosen, correspond to evaluations of the physics-based model.

The monotonic annealing schedule used in the monotonic VBMC is calculated for a total number of iterations $T = 40$, with one cycle $M = 1$ and a parameter $S = 0.5$. However, for the cyclical annealing schedule in the cyclical VBMC, the number of cycles is $M = 5$. The monotonic schedule maximum temperature of fifty is subsequently decreased in each iteration until a minimum temperature of one is reached. The same concept is applied to the cyclical annealing schedule that has five cycles where a pre-set maximum temperature of fifty is subsequently decreased in each iteration until a minimum temperature of one is reached in each cycle.

Throughout the examples it will be shown that the monotonic VBMC and cyclical VBMC require a higher amount of samples evaluations compared to the standard VBMC for problems with low dimensionality (i.e., low number of inferred parameters). This is expected as a total number of iterations $T = 40$ is prescribed for both algorithms, meaning that forty is the lowest number of iterations possible.

4.1 Himmelblau Multi-modal posterior

A multi-modal problem based on [25,49] is introduced in this subsection. The posterior used (4 peaks, 2-dimensional) can be observed on Fig. 3 and it has as its mathematical expression [49] the Himmelblau's function $HB(\theta_1, \theta_2)$:

$$HB(\theta_1, \theta_2) = (\theta_1^2 + \theta_2 - 11)^2 + (\theta_1 + \theta_2^2 - 7)^2 \quad (39)$$

The $HB(\theta_1, \theta_2)$ is frequently used to assess the performance of optimization algorithms.

It has four distinct solutions of local minima at $\{\theta_1, \theta_2\}_1 = \{3, 2\}$, $\{\theta_1, \theta_2\}_2 = \{-2.805, 3.131\}$, $\{\theta_1, \theta_2\}_3 = \{-3.779, -3.283\}$ and $\{\theta_1, \theta_2\}_4 = \{-3.584, -1.848\}$.

The posterior of interest is then defined as follows [25,49]:

$$p(\boldsymbol{\theta} | \mathbf{y}_{\text{obs}}) \propto \exp[-HB(\theta_1, \theta_2)] \quad (40)$$

That ensures that the local minima of $HB(\theta_1, \theta_2)$ become regions of high probability density, producing the 4 peaks shown in Fig. 3. The likelihood function is modelled as the exponential function of $-HB(\theta_1, \theta_2)$, and thus takes the same mathematical form as the posterior [25,49]. The uniform priors $\theta_1 \sim U(-5, 5)$ and $\theta_2 \sim U(-5, 5)$ have been used.

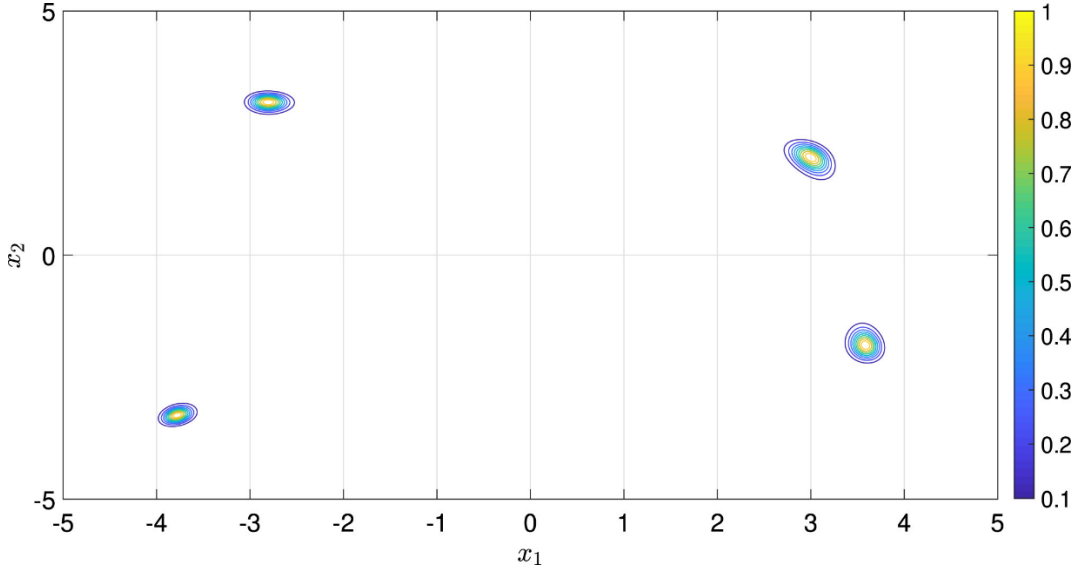


Fig. 3. Contour plot of the Himmelblau's function using eq.(40) taken from [25]. The values of the posterior are given by the numbers on the colour chart.

The results found using the standard VBMC algorithm after running several iterations are illustrated in Fig. 4. The final 1-D and 2-D marginal posterior distributions obtained by the standard VBMC algorithm are shown in Fig. 5. The figures show that only one mode has been found, as due to the nature of the algorithm, the active sampling used is unable to escape from that mode. In other words, the algorithm proceeds to only sample in the

vicinity of that mode due to its exploitation nature. A total of 75 function evaluations were required, and only one mode was found.

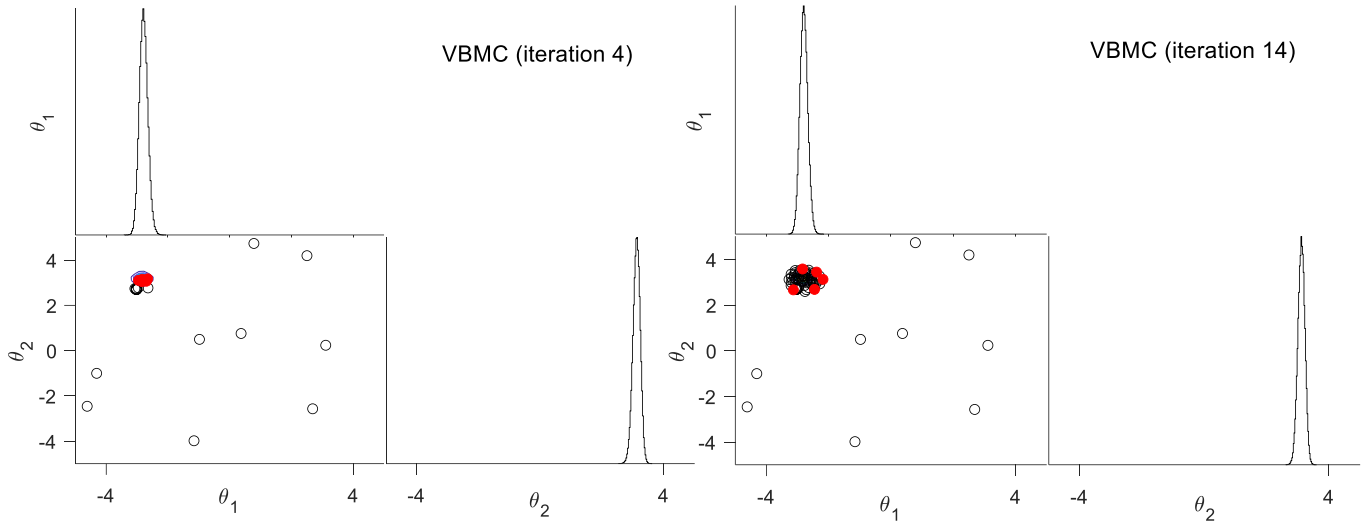


Fig. 4. Resulting 1-D and 2-D marginal posterior distributions from VBMC at 4th and 14th iterations. Red dots indicate samples taken at the current iteration. Black circles indicate samples used for the GP model of the unnormalized posterior at each iteration.

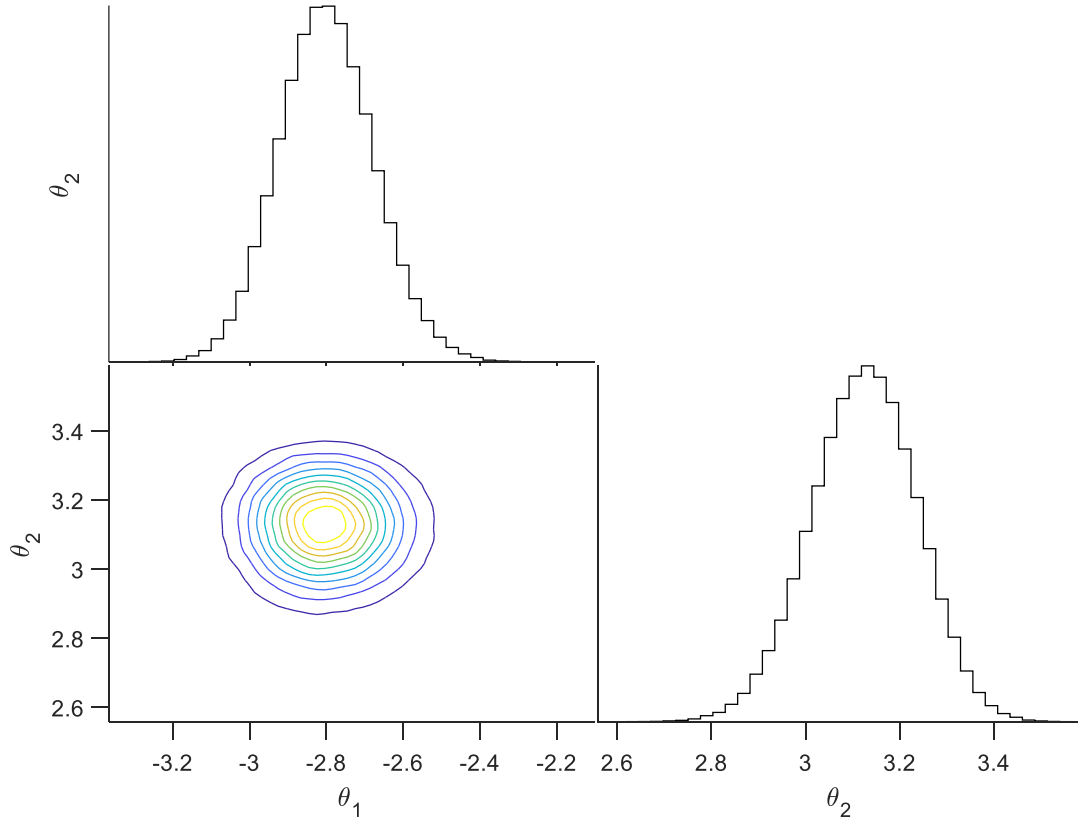


Fig. 5. Final 1-D and 2-D marginal posterior distributions from VBMC algorithm.

The results obtained with the monotonic and the cyclical VBMC algorithm are shown in Fig. 6 and Fig. 7, it is found that the overall results of these two schedules significantly differ.

It can be seen in Fig. 6 that in the monotonic VBMC algorithm, for the first few iterations, the samples are chosen following an exploration approach. In the final iterations of the monotonic algorithm shown in Fig. 7, the samples chosen are close to the two modes found. The resulting refined postulated posterior of the algorithm when using a monotonic annealing schedule is only able to account for two modes. The monotonic VBMC algorithm needs a total of 235 function evaluations to converge to the 2-mode estimated posterior shown in Fig. 8.

It can be seen in Fig. 6, that in the proposed cyclical VBMC algorithm, for the first few iterations, the samples are chosen following both an exploration and an exploitation approach. For the final iterations of the cyclical algorithm, it can be seen in Fig. 7, that the samples chosen are close to the four modes found. The resulting refined postulated posterior of the algorithm, using the cyclical annealing schedule shown in Fig. 8, is able to account for all four modes. A total of 300 function evaluations were needed to converge to the estimated posterior.

The empirical cumulative density functions (ECDFs), shown in Fig. 9 were calculated using samples obtained from both the cyclical VBMC, and the TEMCMC algorithm, applying the function `cdfplot` from Matlab [48]. For the TEMCMC algorithm, the number of samples used to calculate the ECDFs were progressively increased until convergence occurred. It was found that the converged ECDFs obtained by the TEMCMC algorithm, required a much larger number of samples than the cyclical VBMC algorithm.

The computational cost is significantly reduced for the three VBMC algorithms compared to the TEMCMC sampling algorithm, where 5000 evaluations of the likelihood function were needed as shown in [25]. The proposed cyclical VBMC algorithm is the only VBMC variant that is able to find the four modes of the Himmelblau posterior. The numerical results for the Himmelblau multi-modal posterior are summarised in Table 2.

Table 2

Comparison of numerical results for the Himmelblau multi-modal posterior.

Method	N. of samples	N. of Total Iterations for Convergence	N. of modes found
VBMC	75	14	1
Monotonic VBMC	235	46	2
Cyclical VBMC	300	59	4
TEMCMC [37]	5000	5	4

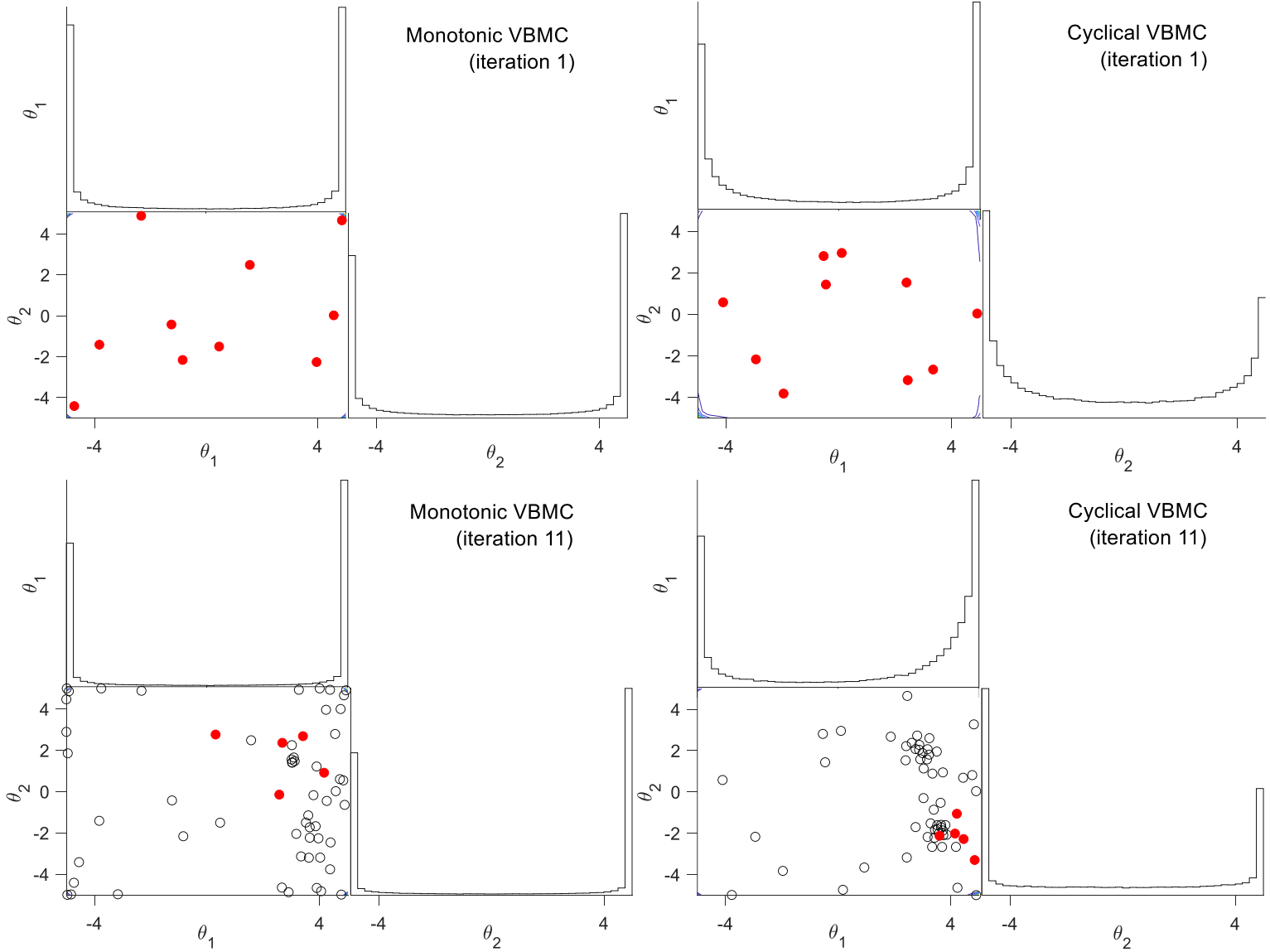


Fig. 6. Resulting 1-D and 2-D marginal posterior distributions from VBMC at 1st and 11th iterations. Red dots indicate samples taken at the current iteration. Black circles indicate samples used for the GP model of the unnormalized posterior at each iteration.

Left: Monotonic annealing schedule; Right: Cyclical Annealing Schedule.

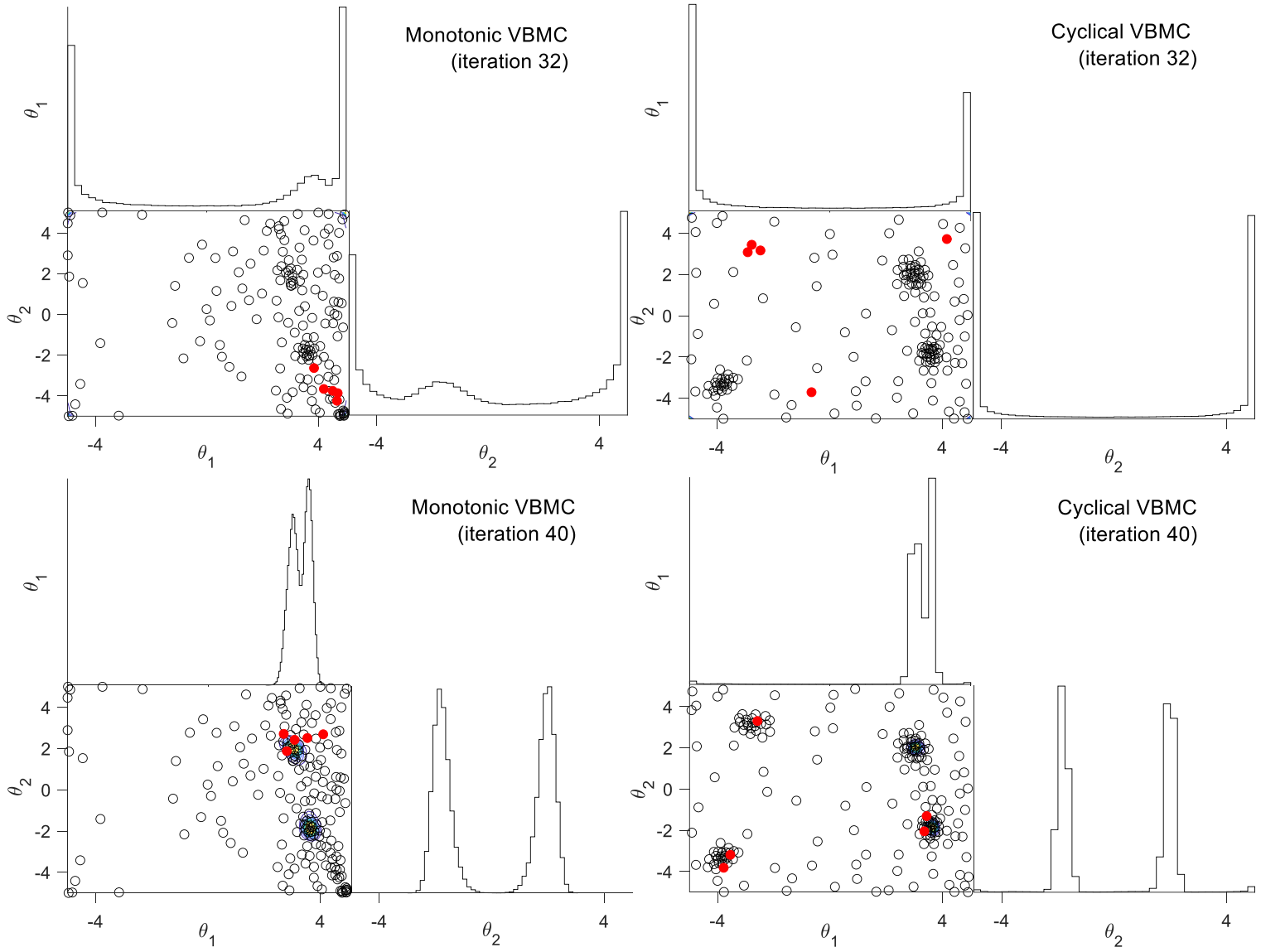


Fig. 7. Resulting 1-D and 2-D marginal posterior distributions from VBMC at 32nd and 40th iterations. Red dots indicate samples taken at the current iteration. Black circles indicate samples used for the GP model of the unnormalized posterior at each iteration. Left: Monotonic annealing schedule; Right: Cyclical Annealing Schedule.

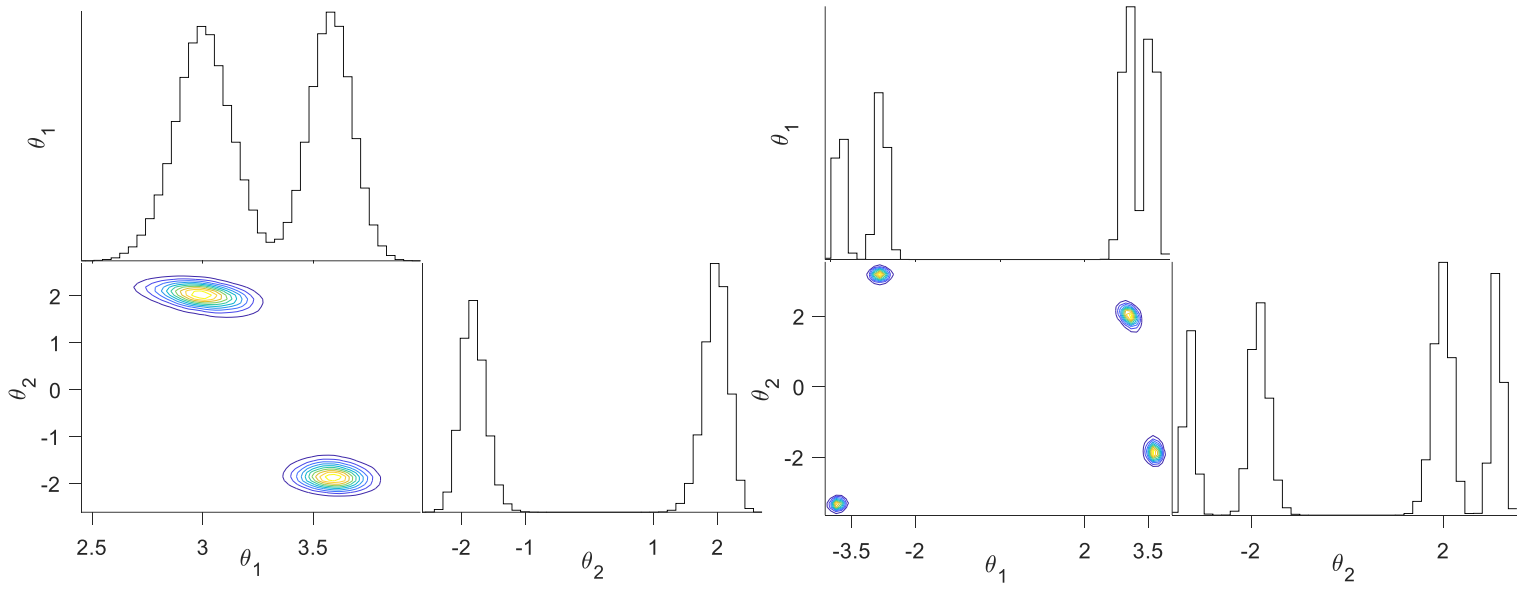


Fig. 8. Final 1-D and 2-D marginal posterior distributions from VBMC algorithm. Left: Monotonic annealing schedule; Right: Cyclical Annealing Schedule.

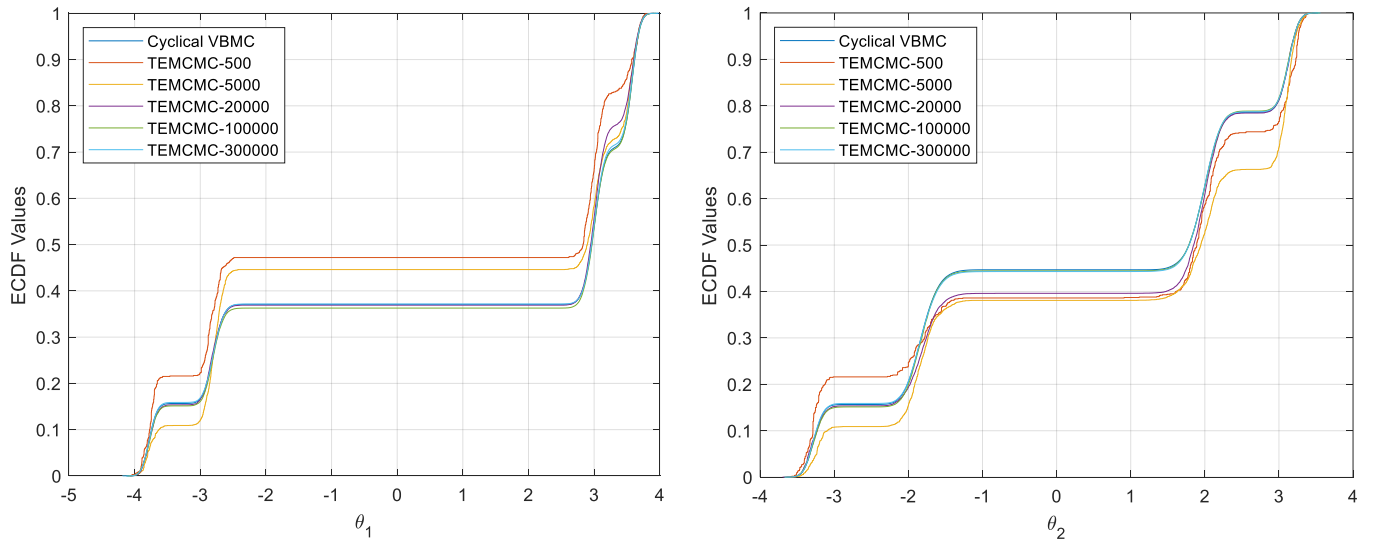


Fig. 9. Marginal ECDFs using Cyclical VBMC and TEMCMC.

4.2 Mass-spring system (multi-modal posterior)

In this example taken from [50], a 2-dimensional multi-modal Bayesian model updating system that may be found in engineering problems, is used to compare the differences in the performance of the aforementioned algorithms. For the purposes of this subsection, the numerical performance will be based on the number of samples used to compute the posterior, the number of modes found in each algorithm and the empirical cumulative density function.

As shown in Fig. 10, a 2-degrees of freedom (2-DoF) system with masses $m_1 = 16.531 \times 10^3 \text{ kg}$, $m_2 = 16.131 \times 10^3 \text{ kg}$ joined by springs with stiffness $k_1 = \bar{k} \theta_1$, $k_2 = \bar{k} \theta_2$, where $\bar{k} = 29.7 \times 10^6 \text{ N/m}$ is defined, and θ_1 and θ_2 are the uncertain parameters to be inferred. For the spring constants, the uniform priors $\theta_1 \sim U(0.01, 3)$ and $\theta_2 \sim U(0.01, 3)$ have been used.

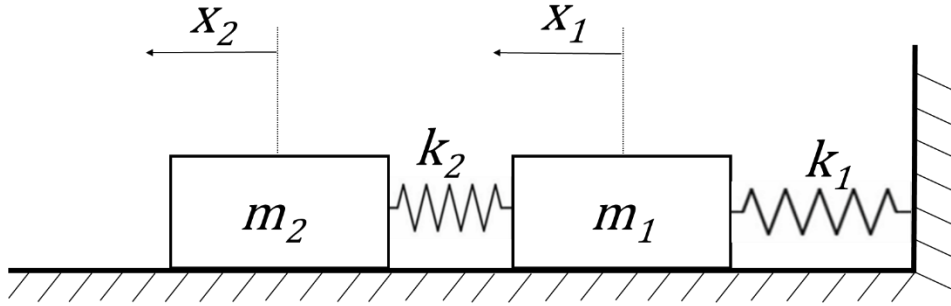


Fig. 10. First mass-spring system.

Two independent likelihood functions are used with standard deviations $\sigma_i = 0.02\omega_i$ (2% of the deterministic values of the natural frequencies) and with means that equal the deterministic values of the natural frequencies.

From Fig. 11, it can be observed that the standard VBMC is only able to find one mode, and that the active sampling is again unable to escape from that mode. The standard algorithm uses a total of 75 function evaluations to obtain the resulting posterior distribution that only accounts for a single mode. The final 1-D and 2-D marginal posterior distributions obtained by the standard VBMC algorithm are shown in Fig. 12.

For the monotonic VBMC algorithm, an exploration phase is shown in the first few iterations. An exploitation phase that samples in the vicinity of the two found modes is illustrated in Fig. 13.

However, for the cyclical VBMC algorithm both exploration and exploitation occur in the early iterations, as shown in Fig. 13. The final 1-D and 2-D marginal posterior distributions obtained by the monotonic and cyclical VBMC algorithm are shown in Fig. 14, where it is possible to observe that both methods account for the two modes.

In Fig. 16 the ECDFs for the cyclical VBMC, monotonic VBMC, and TEMCMC are shown. The resulting ECDFs are found to be similar, with a slight difference observed for the ECDFs obtained from the TEMCMC algorithm.

Table 3 summarises the number of evaluations and iterations needed for the three analysed VBMC algorithms, and the sampling method TEMCMC (Fig. 15). It can be seen that when using the three VBMC algorithms, the computational cost is significantly reduced compared to the TEMCMC sampling algorithm, where 5000 evaluations of the likelihood function were needed to obtain samples from the posterior distribution.

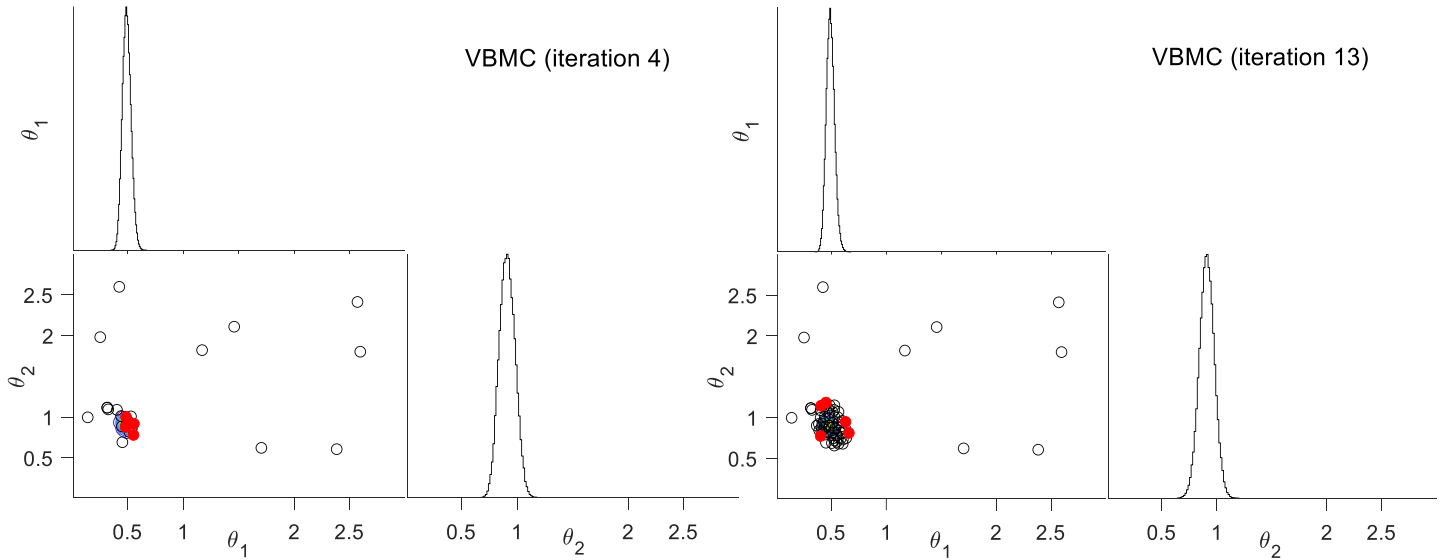


Fig. 11. Resulting 1-D and 2-D marginal posterior distributions from VBMC at 4th and 13th iterations. Red dots indicate samples taken at the current iteration.

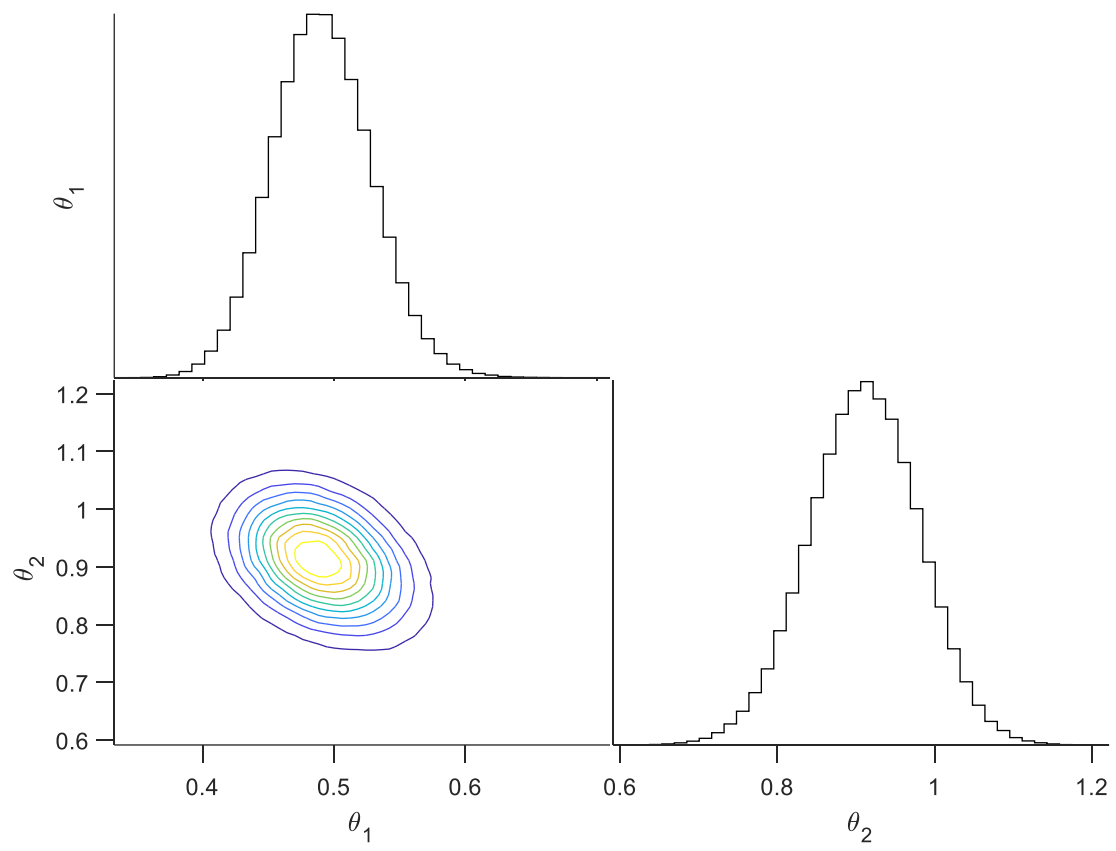


Fig. 12. Final 1-D and 2-D marginal posterior distributions from VBMC algorithm.

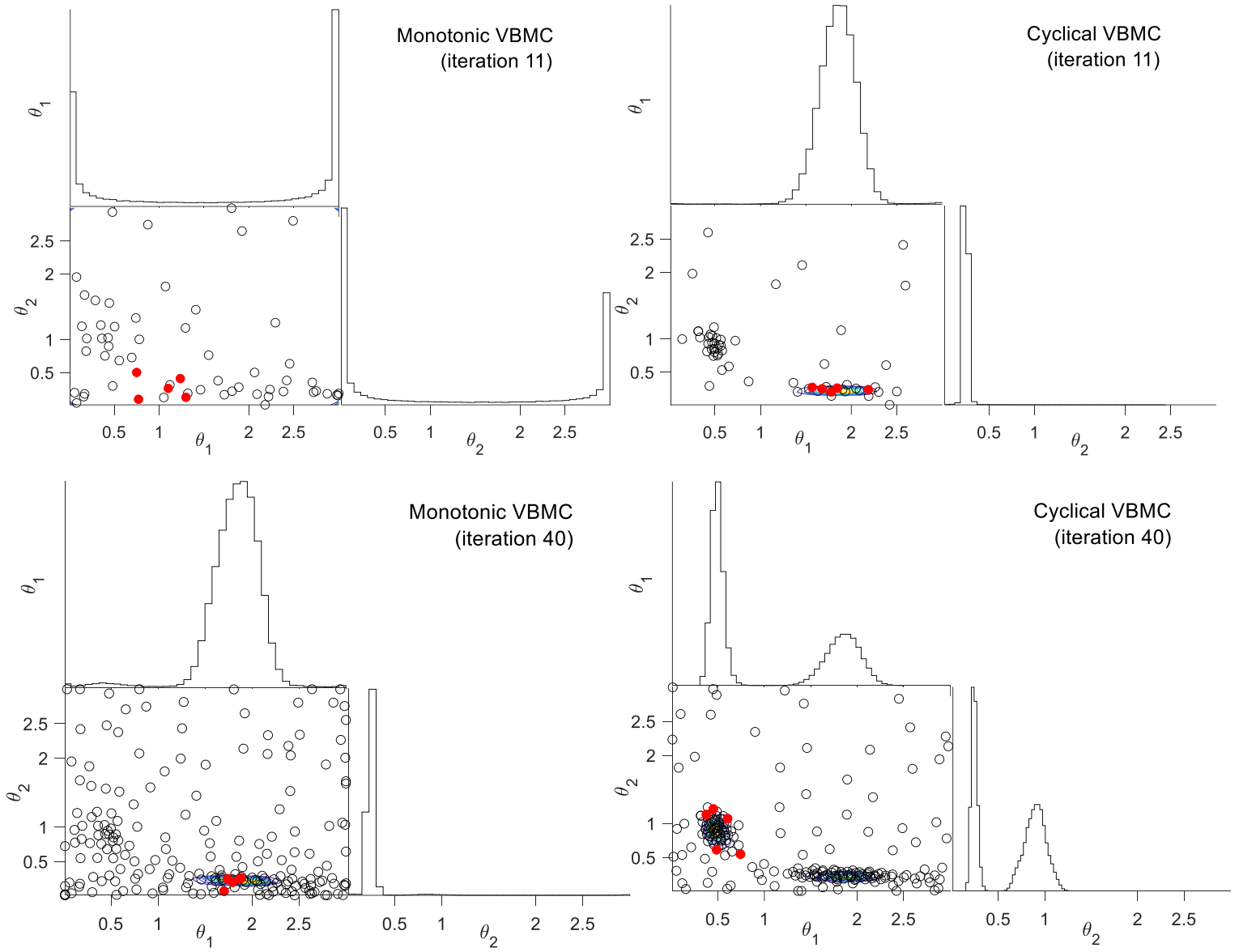


Fig. 13. Resulting 1-D and 2-D marginal posterior distributions from VBMC at 11th and 40th iterations. Red dots indicate samples taken at the current iteration. Black circles indicate samples used for the GP model of the unnormalized posterior at each iteration.

Left: Monotonic annealing schedule; Right: Cyclical Annealing Schedule.

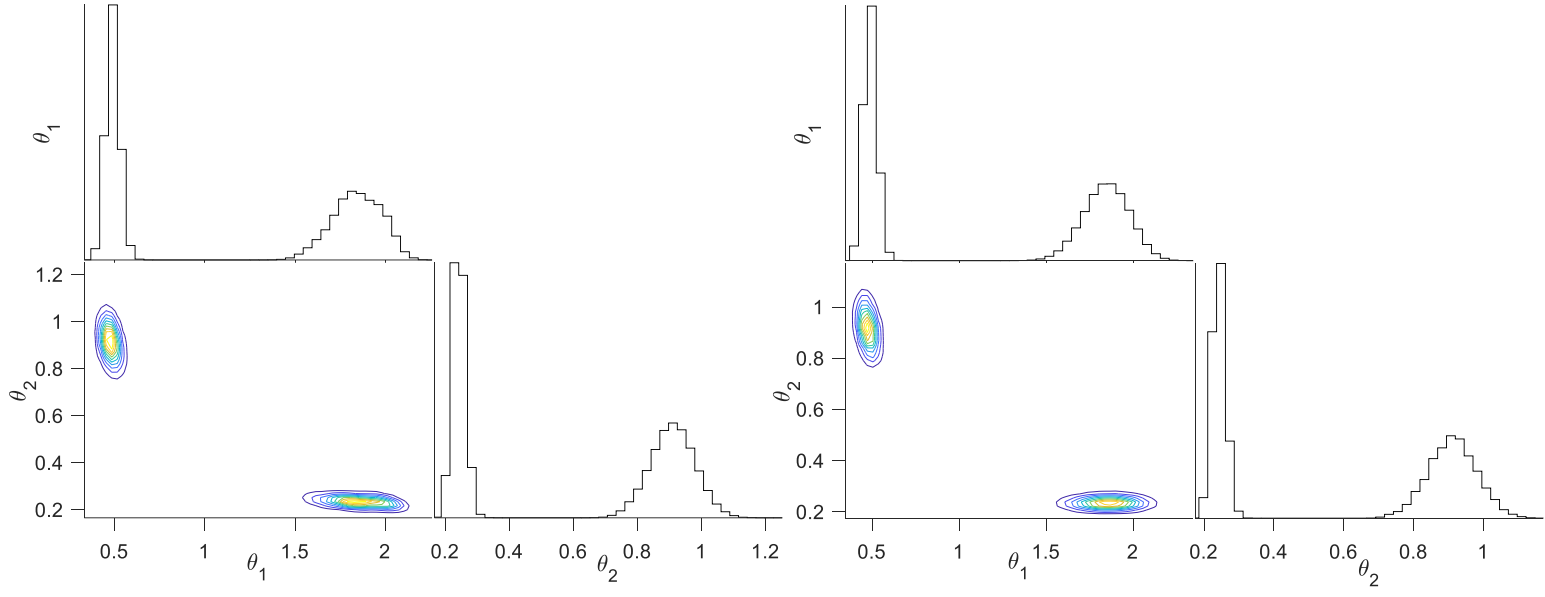


Fig. 14. Final 1-D and 2-D marginal posterior distributions from VBMC algorithm.

Left: Monotonic annealing schedule; Right: Cyclical Annealing Schedule.

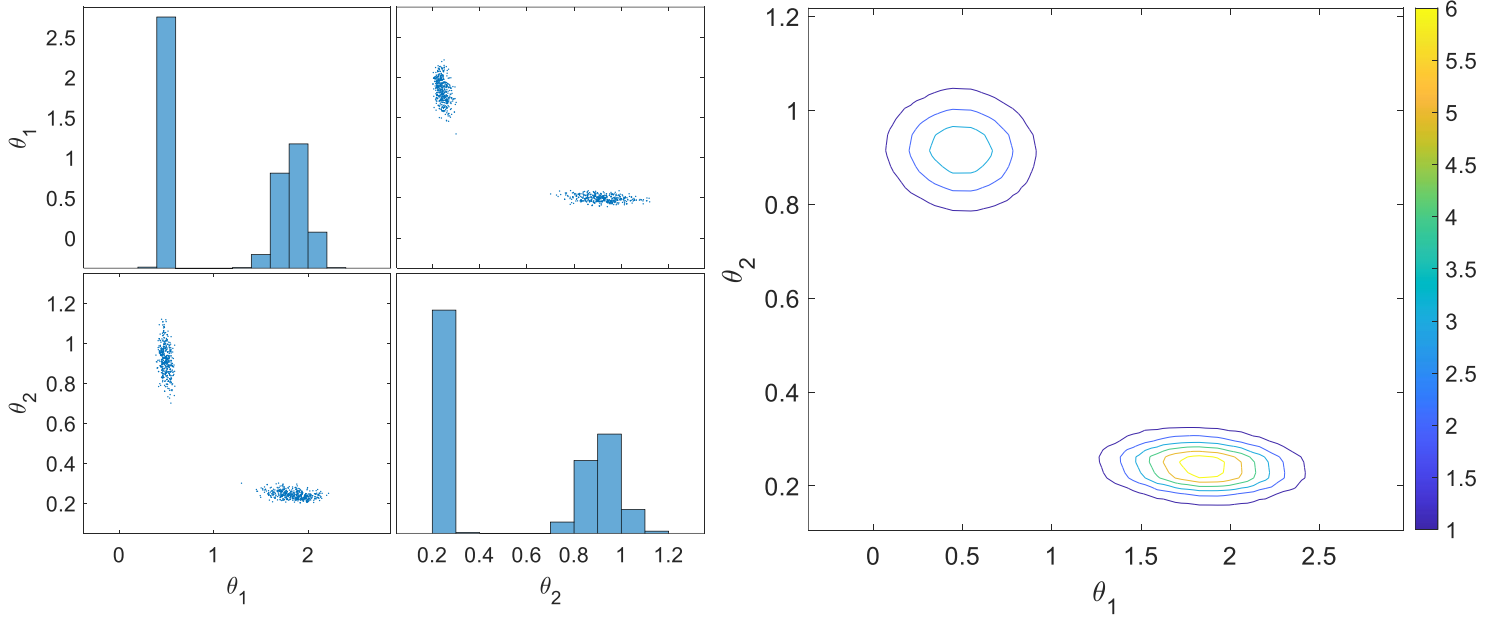


Fig. 15. Scatterplot and 2-D posterior distribution from TEMCMC algorithm. The values of the 2-D posterior are given by the numbers on the colour chart.

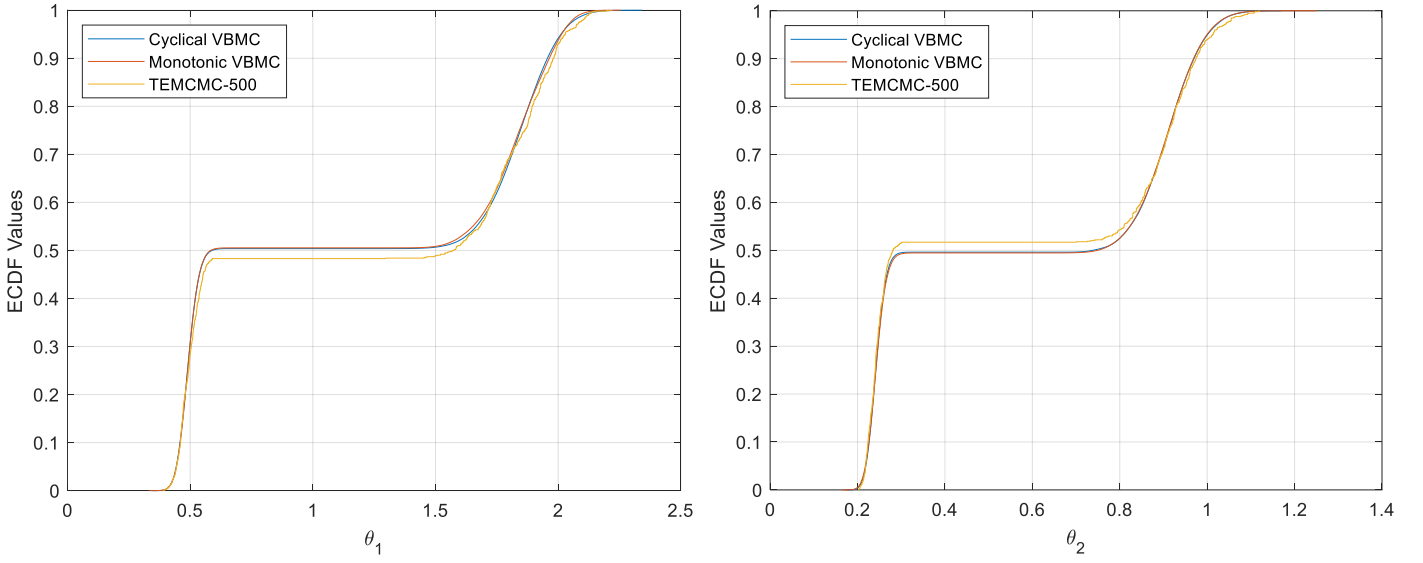


Fig. 16. Marginal ECDFs using Cyclical VBMC, Monotonic VBMC and TEMCMC.

Table 3

Comparison of numerical results for the mass-spring (multi-modal) system.

Method	N. of samples	N. of Total Iterations for Convergence	N. of modes found
VBMC	70	13	1
Monotonic VBMC	275	54	2
Cyclical VBMC	260	51	2
TEMCMC	5000	5	2

4.3 Mass-spring system (unimodal posterior)

In this example taken from [25], for a 4-dimensional Bayesian model updating system, the two Degrees-of-Freedom (DoF) system shown in Fig. 17 is used to compare the performances of all algorithms.

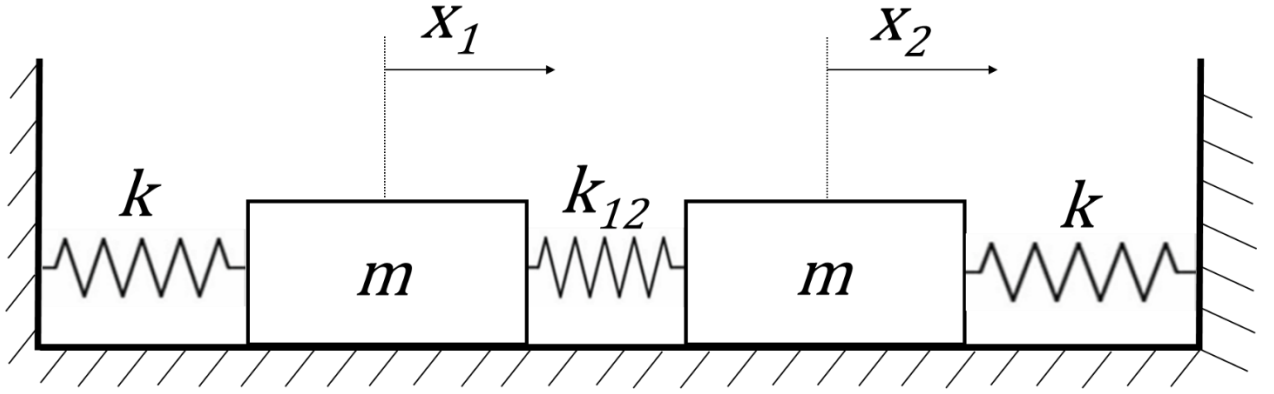


Fig. 17. Second mass-spring system.

The 2-DoF system has equal masses $m = 0.5\text{kg}$ attached to edge springs with stiffness $k = 0.6\text{N/m}$, and the stiffness of the spring between the two masses is $k_{12} = 1\text{N/m}$.

The natural frequencies that correspond to the specified properties of the two-degree-of freedom system are given by [25]:

$$\hat{\omega}_1 = \sqrt{\frac{k}{m}} \quad (41)$$

$$\hat{\omega}_2 = \sqrt{\frac{k + 2k_{12}}{m}} \quad (42)$$

The values of the natural frequencies $\hat{\omega}_1$ and $\hat{\omega}_2$ are corrupted with noise as shown below [25]:

$$\omega_1 = \hat{\omega}_1 + \varepsilon_1 \quad (43)$$

$$\omega_2 = \hat{\omega}_2 + \varepsilon_2 \quad (44)$$

Where ε_1 and ε_2 are the noise terms, that follow Gaussian statistical distributions. The mean of both Gaussian distributions is 0Hz , and their standard deviations are respectively $\sigma_1 = 0.1\hat{\omega}_1 = 0.110\text{Hz}$ and $\sigma_2 = 0.1\hat{\omega}_2 = 0.228\text{Hz}$. The likelihood function is then given by the equation below [25]:

$$P(y_{obs} | \theta) = \prod_{n=1}^{15} \frac{1}{2\pi\sigma_1\sigma_2} \exp \left[-\frac{(\omega_{1,n} - \hat{\omega}_1)^2}{2\sigma_1^2} - \frac{(\omega_{2,n} - \hat{\omega}_2)^2}{2\sigma_2^2} \right] \quad (45)$$

In this example, the parameters $\{k, k_{12}, \sigma_1, \sigma_2\} \equiv \{\theta_1, \theta_2, \theta_3, \theta_4\}$ are assumed to be unknown. The uniform priors $k \sim U(0.1, 4)$ [N/m] and $k_{12} \sim U(0.1, 4)$ [N/m] have been used for the stiffnesses. The prior uniforms taken for the standard deviations σ_1 and σ_2 are $\sigma_1 \sim U(10^{-5}, 1)$ [Hz] and $\sigma_2 \sim U(10^{-5}, 1)$ [Hz]. The posterior probability density functions of the parameters is updated using the ‘experimental measurements’, for this example, the fifteen individual experimental ‘measurements’ of ω_1 and ω_2 used are found in [25].

The final posterior using 1D and 2D marginal distributions are shown in Fig. 18, Fig. 19 and Fig. 20.

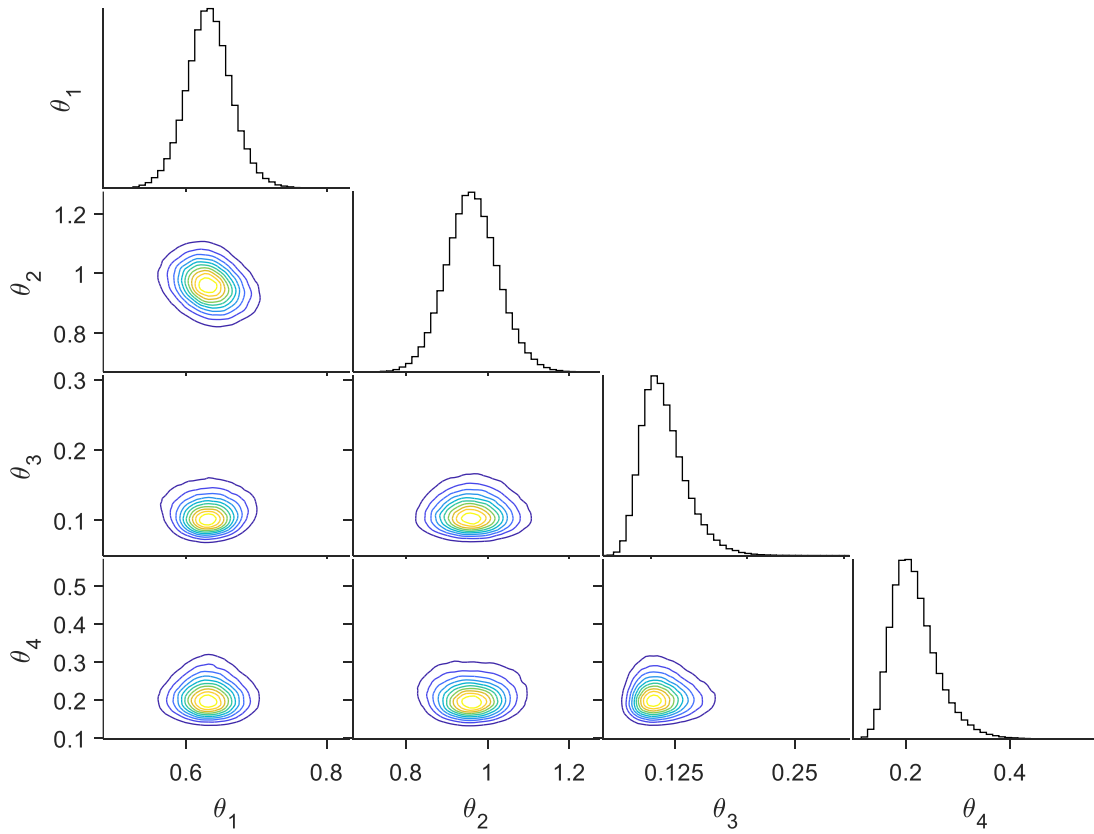


Fig. 18. Final 1-D and 2-D marginal posterior distributions from standard VBMC algorithm.

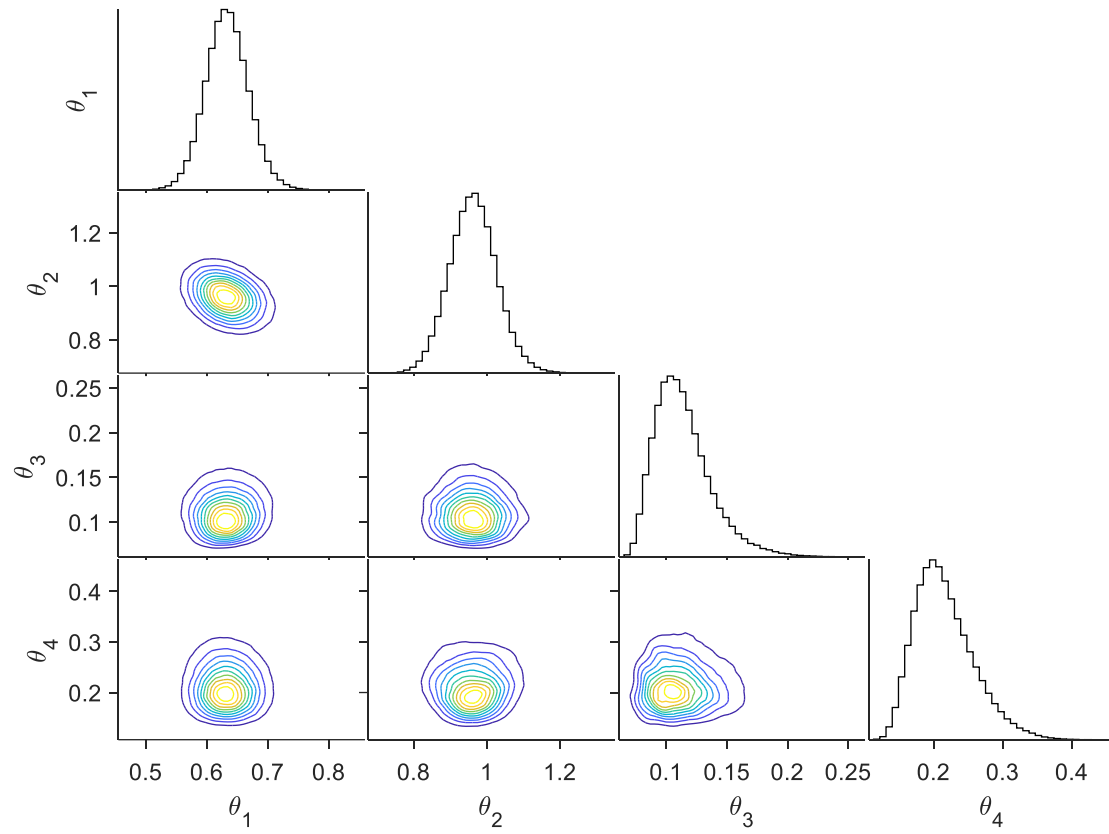


Fig. 19. Final 1-D and 2-D marginal posterior distributions from monotonic VBMC algorithm.

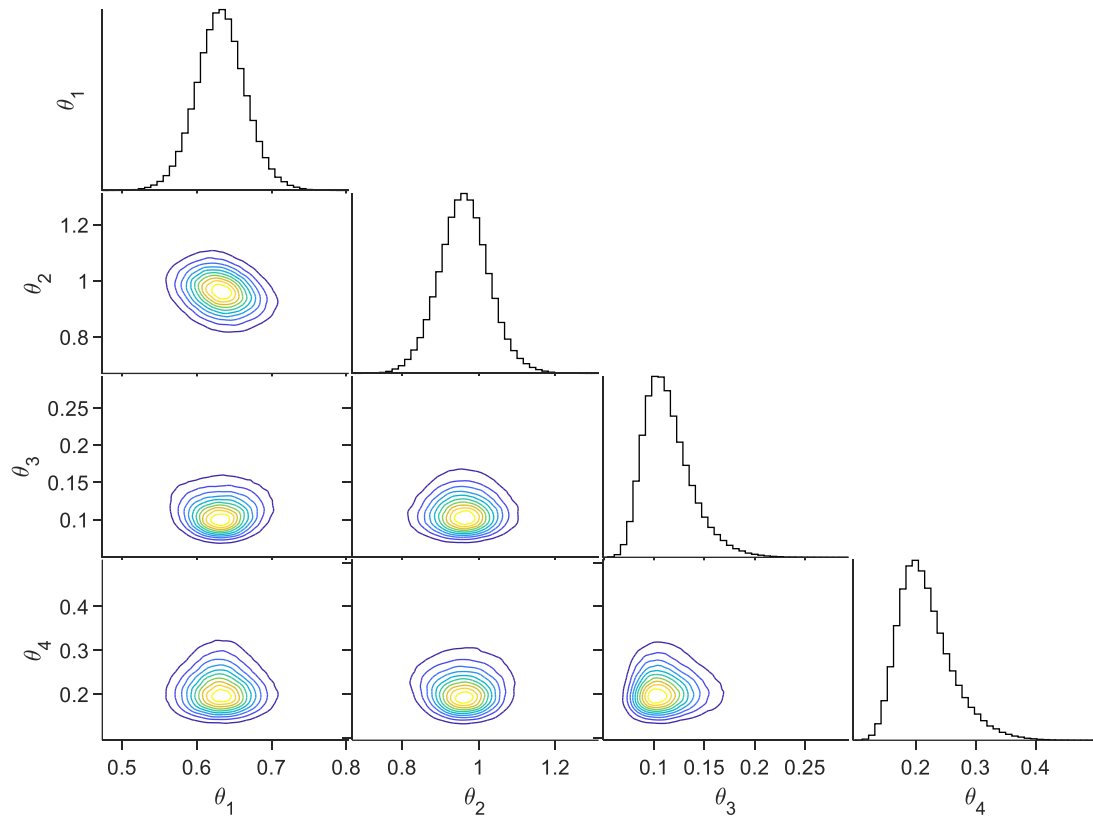


Fig. 20. Final 1-D and 2-D marginal posterior distributions from cyclical VBMC algorithm.

Table 4

Comparison of numerical results for the mass-spring system.

Method	Sample Mean	Sample C.O.V [%]	N. of samples	N. of Total Iterations for Convergence
VBMC	$\begin{bmatrix} 0.633\text{N/m} \\ 0.962\text{N/m} \\ 0.114\text{Hz} \\ 0.217\text{Hz} \end{bmatrix}$	$\begin{bmatrix} 5.21 \\ 6.67 \\ 20.66 \\ 20.82 \end{bmatrix}$	220	43
Monotonic VBMC	$\begin{bmatrix} 0.633\text{N/m} \\ 0.963\text{N/m} \\ 0.114\text{Hz} \\ 0.216\text{Hz} \end{bmatrix}$	$\begin{bmatrix} 5.68 \\ 6.73 \\ 20.70 \\ 19.71 \end{bmatrix}$	265	52
Cyclical VBMC	$\begin{bmatrix} 0.632\text{N/m} \\ 0.962\text{N/m} \\ 0.114\text{Hz} \\ 0.217\text{Hz} \end{bmatrix}$	$\begin{bmatrix} 5.34 \\ 6.85 \\ 21.32 \\ 20.85 \end{bmatrix}$	260	51
TEMCMC [25]	$\begin{bmatrix} 0.625\text{N/m} \\ 1.013\text{N/m} \\ 0.121\text{Hz} \\ 0.229\text{Hz} \end{bmatrix}$	$\begin{bmatrix} 5.67 \\ 6.80 \\ 17.25 \\ 26.15 \end{bmatrix}$	5000	5
True Values	$\begin{bmatrix} 0.6\text{N/m} \\ 1\text{N/m} \\ 0.11\text{Hz} \\ 0.228\text{Hz} \end{bmatrix}$	-	-	-

Table 4, for a 4D dimensional problem, shows that a significant lower amount of model evaluations is needed for the three VMBC approaches to obtain similar results to the obtained with the TEMCMC algorithm. The results obtained using the TEMCMC algorithm are taken from [25].

4.4 Coupled-Beam structure

In this example, a coupled beam structure is used to compare the performance of the previously mentioned algorithms. The two beams are connected in two points along their length by two ensembles, each consisting of one shear, one rotational and one translational spring as shown in Fig. 21. This case study has been chosen as it may be used to illustrate the practical cases in which the physical properties of the fixtures that attach components in a structure exhibit uncertainty. The uncertainty of those physical properties may be caused by the variability of the manufacturing processes, the assembly of the fixtures and their boundary conditions.

In particular, the parameters to be inferred are the rotational spring stiffness $k_2 \equiv \theta_1$ and the magnitude of the shear spring stiffness $k_3 \equiv \theta_2$. A prior distribution is assigned to each of these two parameters. Uniform priors were used for the stiffness $k_2 \sim U(200, 1000)$ [Nm/rad] of both rotational springs, and for the stiffness $k_3 \sim U(0.1, 30)$ [MN/m] of both shear springs.

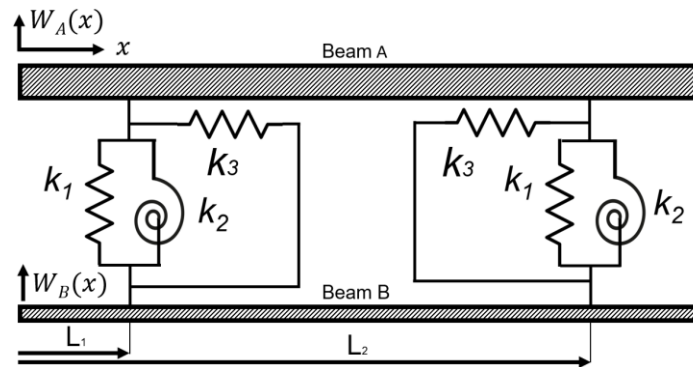


Fig. 21. Theoretical model of a coupled beam structure.

Table 5 describes the material and geometric characteristics of the structure used.

Table 5

Material and geometric characteristics of the coupled beam.

	Length [m]	Width [mm]	Thickness [mm]	Density [Kg/m ³]	Youngs' modulus [GPa]
Beam A	0.6	25	6	7800	210
Beam B	0.6	25	3	7800	210
L_1 and L_2 (Length to springs)	L_1 [mm]		L_2 [mm]		
	20		20		
Springs	k_1 [MN/m]		k_2 [Nm/rad]		k_3 [MN/m]
	100		500		10

The natural frequencies of the coupled beam were calculated using the values on Table 5 and the results are shown on Table 6.

Table 6

Natural frequencies of the coupled beam structure.

$freq_1$	$freq_2$	$freq_3$	$freq_4$	$freq_5$	$freq_6$	$freq_7$	$freq_8$
[Hz]	[Hz]	[Hz]	[Hz]	[Hz]	[Hz]	[Hz]	[Hz]
16.0	50.2	92.8	134.6	245.3	260.7	428.0	478.6

A Finite Element (FE) model is used to calculate the natural frequencies of the coupled beam structure. The developed FE code is based on a two-dimensional Euler-Bernoulli beam model. This is discretized uniformly using 200 Euler-Bernoulli beam FEs with 2 degrees of freedom per node.

Eight independent likelihood functions with standard deviations $\sigma_i = 0.02 \text{freq}_i$ (2% of the deterministic values of the natural frequencies) and with means that equal the deterministic values of the natural frequencies are used.

Fig. 22, Fig. 23, Fig. 24 show the final 1-D and 2-D marginal posterior distributions obtained from the algorithms. In Fig. 25, a scatterplot of the samples obtained and the 2-D posterior distribution from the TEMCMC algorithm are shown.

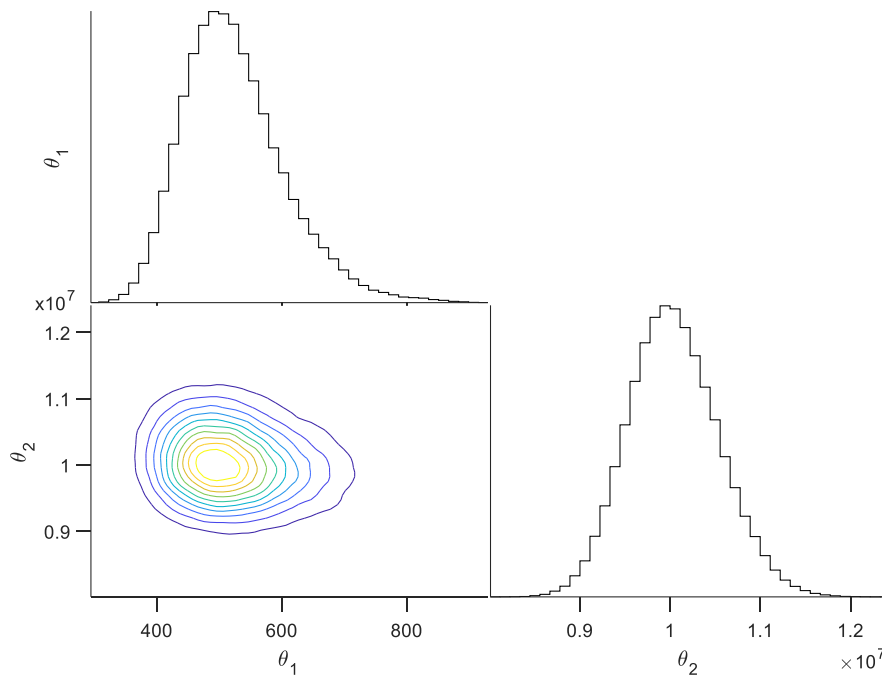


Fig. 22. Final 1-D and 2-D marginal posterior distributions from VBMC algorithm.

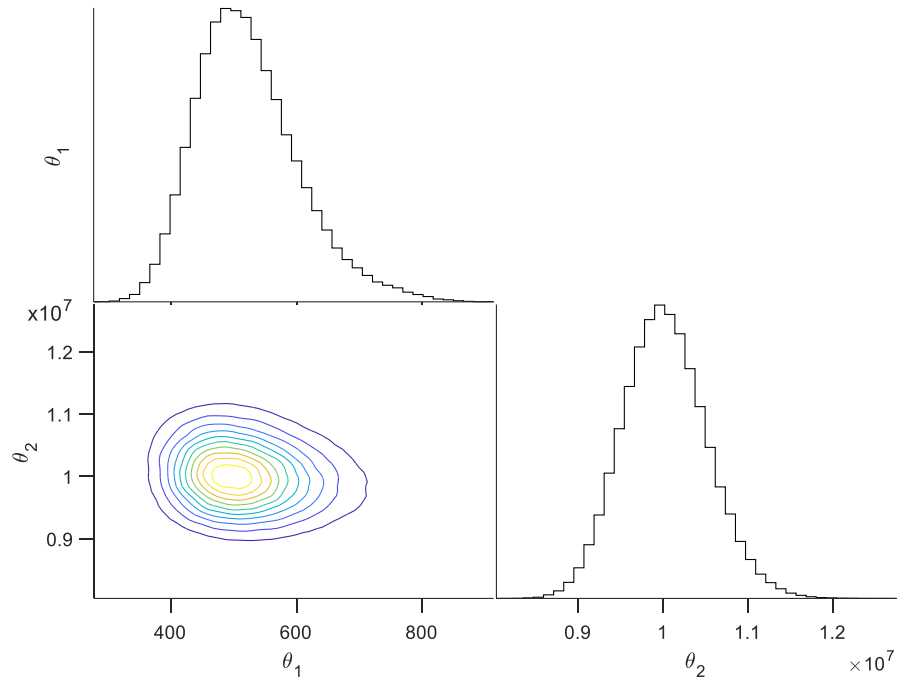


Fig. 23. Final 1-D and 2-D marginal posterior distributions from monotonic VBMC algorithm.

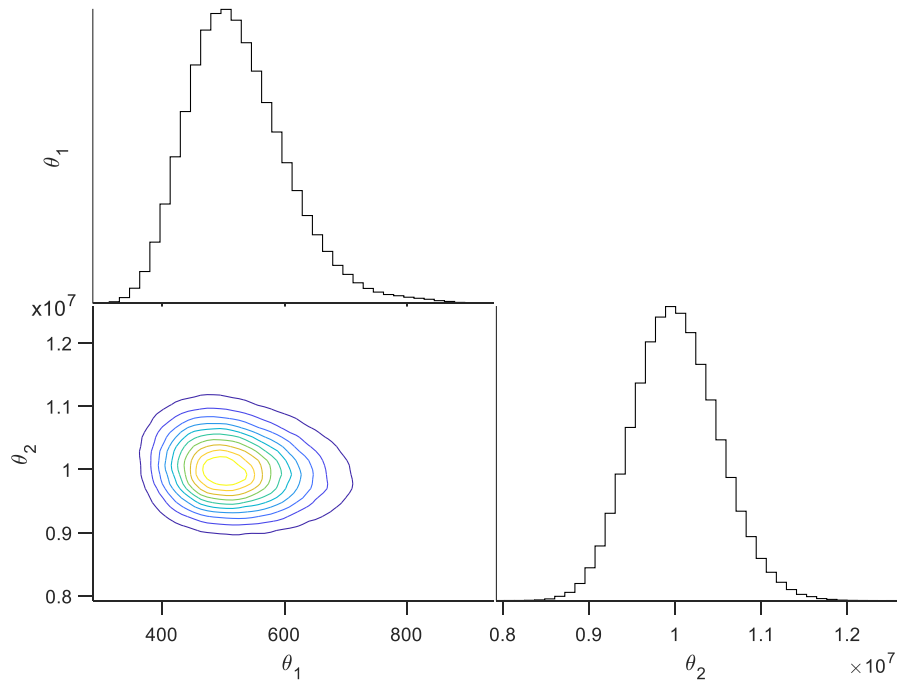


Fig. 24. Final 1-D and 2-D marginal posterior distributions from cyclical VBMC algorithm.

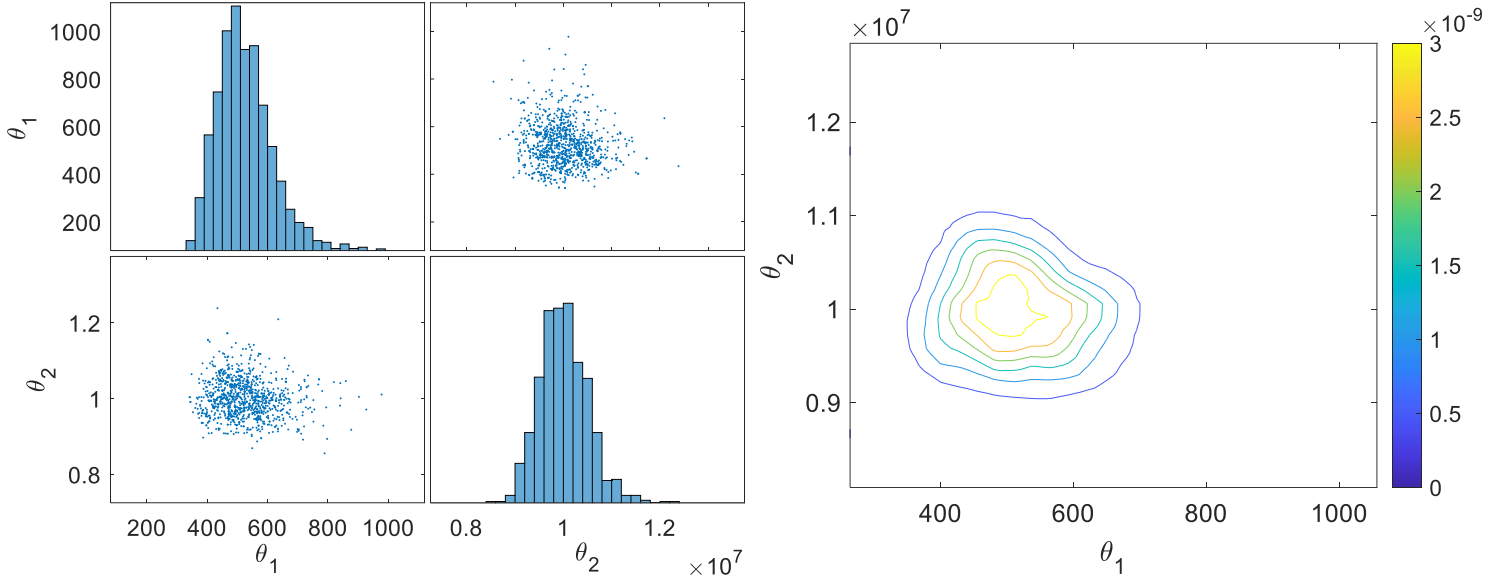


Fig. 25. Scatterplot and 2-D posterior distribution from TEMCMC algorithm. The values of the 2-D posterior are given by the numbers on the colour chart.

Table 7 compares the results obtained using the three VBMC approaches and TEMCMC. It can be seen that for a significantly lower amount of model evaluations, all the three VBMC algorithms show similar results to the TEMCMC algorithm.

Table 7

Comparison of numerical results for the coupled-beam structure.

Method	Mean	C.O.V. [%]	N. of samples	N. of Total Iterations for Convergence
VBMC	$\begin{bmatrix} 523.2\text{Nm/rad} \\ 1.004\text{e}+07 \text{ N/m} \end{bmatrix}$	$\begin{bmatrix} 15.7 \\ 4.96 \end{bmatrix}$	75	14
Monotonic VBMC	$\begin{bmatrix} 523.2\text{Nm/rad} \\ 1.003\text{e}+07 \text{ N/m} \end{bmatrix}$	$\begin{bmatrix} 15.7 \\ 4.92 \end{bmatrix}$	265	52
Cyclical VBMC	$\begin{bmatrix} 524.5\text{Nm/rad} \\ 1.002\text{e}+07 \text{ N/m} \end{bmatrix}$	$\begin{bmatrix} 15.7 \\ 4.92 \end{bmatrix}$	260	51
TEMCMC	$\begin{bmatrix} 525.2\text{Nm/rad} \\ 1.001\text{e}+07 \text{ N/m} \end{bmatrix}$	$\begin{bmatrix} 17.3 \\ 4.94 \end{bmatrix}$	5000	5

True Values	$\begin{bmatrix} 500\text{Nm/rad} \\ 1\text{e}+07\text{ N/m} \end{bmatrix}$	-	-	-
-------------	---	---	---	---

4.5 Discussion of results

The results obtained for the examples illustrated in section 4 indicate that:

The use of the three VBMC algorithms led to a sharp reduction in the number of function evaluations to be carried out to obtain an accurate unimodal posterior, compared to the case where the TEMCMC sampling method is used. For low unimodal dimensional Bayesian updating problems the standard VBMC algorithm produces accurate results with the lowest number of function evaluations.

It is also shown that the standard VBMC algorithm, for the multi-modal problems analysed, gets stuck at the initially found mode, as due to the nature of the algorithm, the active sampling used is unable to escape from that mode. In other words, the algorithm proceeds to only sample in the vicinity of that found mode due to its exploitation nature. A better approximation of the posterior may have been found if a higher number of function evaluations had been used for the initial training set, as that would have meant a better exploration of regions with high probability density. The disadvantage of running a higher number of function evaluations would be that as no guided exploration is used, a significant number of those function evaluations performed would be wasted.

To overcome the above explained issue, an annealing schedule was introduced into the VBMC algorithm. The purpose of this annealing schedule is to obtain a better representation of the posterior through the introduction of an exploration phase with improved target guidance. In the examples of section 4, the performance for the approximation of multi-modal posteriors of this proposed cyclical VBMC was compared to the performance of the monotonic VBMC.

For the two multi-modal examples, at the start of each cycle, the samples chosen to be evaluated follow an exploratory path. Then, an exploitation phase where samples are chosen to be evaluated at the vicinity of the high probability density regions found during the exploration phase occurs. The main advantage of the cyclical schedule is that it gradually improves convergence by reopening paths and by leveraging on the previous cycles as warm re-starts. However, the reopening of paths does not appear for the

monotonic VBMC algorithm. When the monotonic VBMC algorithm is used, the paths are formed throughout the iterations, but they are not reopened, meaning that once the exploration phase has finished, exploitation of the previously found regions of high probability density occurs.

In both multi-modal examples, it was found that to obtain ECDFs of similar accuracy, the cyclical VBMC algorithm required a significantly lower amount of function evaluations of the model compared to the TEMCMC algorithm. This finding may be of great interest for methods that require the evaluation of cumulative density functions, such as reliability analysis techniques.

For high dimensional Bayesian updating problems, the three VBMC algorithms explored may be used to obtain accurate results with a comparable number of function evaluations. Overall, the cyclical VBMC algorithm shows a good balance between exploitation and exploration compared to the monotonic and standard VBMC algorithms. The best performance of the cyclical VBMC algorithm occurs for multi-modal Bayesian updating problems.

5 Conclusions

In this paper, an approach based on variational inference for the estimation of the posterior distribution of the latent parameters of a physics-based model, given available data, has been proposed. The numerical examples illustrate that this model updating approach is an effective alternative to current sampling approaches (TEMCMC), as the number of function evaluations required to obtain an estimate of the posterior distribution is greatly reduced. It can also be seen that the reduction of function evaluations has little impact on the accuracy of the approximated posterior. The proposed cyclical VBMC approach yields a non-parametric estimation of the posterior distribution of the identified parameters by combining the active-sampling Bayesian quadrature with a Gaussian-process based variational inference. The proposed approach can capture complex smooth posteriors as it uses a multivariate Gaussian mixture postulated posterior. Variational whitening is also used in this proposed approach for a more accurate posterior approximation.

This paper introduces the cyclical VBMC algorithm that overcomes the constraints raised by poor initializations when the number of model runs that can be explored is small. This

is done employing an artificial temperature parameter that anneals the unnormalized posterior, improving the mode coverage and exploration abilities of the procedure. The advantages of the cyclical annealing schedule are shown by comparing it to the original algorithm and the monotonic annealing scheduling. These advantages are clearly evident for the examples with multi-modal posteriors. It should also be noted, that although the standard VBMC has a better performance in low unimodal dimensional posteriors in terms of the number of functions evaluated, it is unable to properly manage multi-modal posteriors. However, the proposed cyclical VBMC algorithm has a greater exploration ability to deal effectively with multi-modal posteriors.

Acknowledgements

Felipe Igea and Alice Cicirello thank the EPSRC and Schlumberger for an industrial CASE postgraduate studentship.

References

- [1] A. Lye, A. Cicirello, E. Patelli, Sampling methods for solving Bayesian model updating problems: A tutorial, *Mechanical Systems and Signal Processing*. 159 (2021) 107760. <https://doi.org/10.1016/j.ymssp.2021.107760>.
- [2] L.S. Katafygiotis, J.L. Beck, Updating Models and Their Uncertainties. II: Model Identifiability, *Journal of Engineering Mechanics*. 124 (1998) 463–467. [https://doi.org/10.1061/\(ASCE\)0733-9399\(1998\)124:4\(463\)](https://doi.org/10.1061/(ASCE)0733-9399(1998)124:4(463)).
- [3] J.L. Beck, L.S. Katafygiotis, Updating Models and Their Uncertainties. I: Bayesian Statistical Framework, *Journal of Engineering Mechanics*. 124 (1998) 455–461. [https://doi.org/10.1061/\(ASCE\)0733-9399\(1998\)124:4\(455\)](https://doi.org/10.1061/(ASCE)0733-9399(1998)124:4(455)).
- [4] E. Simoen, G. de Roeck, G. Lombaert, Dealing with uncertainty in model updating for damage assessment: A review, *Mechanical Systems and Signal Processing*. 56 (2015) 123–149. <https://doi.org/10.1016/j.ymssp.2014.11.001>.
- [5] J.K. Kruschke, Markov Chain Monte Carlo, in: *Doing Bayesian Data Analysis*, Elsevier, 2015: pp. 143–191. <https://doi.org/10.1016/B978-0-12-405888-0.00007-6>.

- [6] D.M. Blei, A. Kucukelbir, J.D. McAuliffe, Variational Inference: A Review for Statisticians, *Journal of the American Statistical Association*. 112 (2017) 859–877. <https://doi.org/10.1080/01621459.2017.1285773>.
- [7] W.K. Hastings, Monte carlo sampling methods using Markov chains and their applications, *Biometrika*. 57 (1970) 97–109. <https://doi.org/10.1093/biomet/57.1.97>.
- [8] W.R. Gilks, P. Wild, Adaptive Rejection Sampling for Gibbs Sampling, *Applied Statistics*. 41 (1992) 337. <https://doi.org/10.2307/2347565>.
- [9] S. Chib, Chapter 57 Markov chain Monte Carlo methods: computation and inference, in: *Handbook of Econometrics*, Elsevier, 2001: pp. 3569–3649. [https://doi.org/10.1016/S1573-4412\(01\)05010-3](https://doi.org/10.1016/S1573-4412(01)05010-3).
- [10] D.P. Kingma, T. Salimans, R. Jozefowicz, X. Chen, I. Sutskever, M. Welling, Improving Variational Inference with Inverse Autoregressive Flow, *Advances in Neural Information Processing Systems*. (2016) 4743–4751. <http://arxiv.org/abs/1606.04934> (accessed May 12, 2021).
- [11] A. Kucukelbir, D. Tran, R. Ranganath, A. Gelman, D.M. Blei, Automatic Differentiation Variational Inference, *Journal of Machine Learning Research*. 18 (2016) 1–45. <http://arxiv.org/abs/1603.00788> (accessed May 12, 2021).
- [12] S. Gershman, M. Hoffman, D. Blei, Nonparametric variational inference, *Proceedings of the 29th International Conference on Machine Learning, ICML 2012*. 1 (2012) 663–670. <http://arxiv.org/abs/1206.4665> (accessed May 12, 2021).
- [13] T. Campbell, X. Li, Universal Boosting Variational Inference, *ArXiv*. (2019). <http://arxiv.org/abs/1906.01235> (accessed May 12, 2021).
- [14] L. Acerbi, Variational Bayesian Monte Carlo, *Advances in Neural Information Processing Systems*. 2018-December (2018) 8213–8223. <http://arxiv.org/abs/1810.05558> (accessed May 12, 2021).
- [15] L. Acerbi, Variational Bayesian Monte Carlo with Noisy Likelihoods, *Advances in Neural Information Processing Systems* 34. (2020). <http://arxiv.org/abs/2006.08655> (accessed May 12, 2021).
- [16] C.E. Rasmussen, Z. Ghahramani, Bayesian Monte Carlo, n.d. <http://www.gatsby.ucl.ac.uk> (accessed May 13, 2021).
- [17] A. O’Hagan, Bayes-Hermite quadrature, *Journal of Statistical Planning and Inference*. 29 (1991) 245–260. [https://doi.org/10.1016/0378-3758\(91\)90002-V](https://doi.org/10.1016/0378-3758(91)90002-V).

- [18] C.E. Rasmussen, C.K.I. Williams, Gaussian Processes for Machine Learning, n.d. www.GaussianProcess.org/gpml (accessed May 15, 2021).
- [19] P. Ni, J. Li, H. Hao, Q. Han, X. Du, Probabilistic model updating via variational Bayesian inference and adaptive Gaussian process modeling, *Computer Methods in Applied Mechanics and Engineering*. 383 (2021) 113915. <https://doi.org/10.1016/J.CMA.2021.113915>.
- [20] E.G. Ryan, C.C. Drovandi, J.M. McGree, A.N. Pettitt, A Review of Modern Computational Algorithms for Bayesian Optimal Design, *International Statistical Review*. 84 (2016) 128–154. <https://doi.org/10.1111/insr.12107>.
- [21] Z. Xu, Q. Liao, Gaussian process based expected information gain computation for bayesian optimal design, *Entropy*. 22 (2020) 258. <https://doi.org/10.3390/e22020258>.
- [22] X. Huan, Y.M. Marzouk, Simulation-based optimal Bayesian experimental design for nonlinear systems, *Journal of Computational Physics*. 232 (2013) 288–317. <https://doi.org/10.1016/j.jcp.2012.08.013>.
- [23] G. Capellari, E. Chatzi, S. Mariani, Structural Health Monitoring Sensor Network Optimization through Bayesian Experimental Design, *ASCE-ASME Journal of Risk and Uncertainty in Engineering Systems, Part A: Civil Engineering*. 4 (2018) 04018016. <https://doi.org/10.1061/ajrua6.0000966>.
- [24] C. Argyris, S. Chowdhury, V. Zabel, C. Papadimitriou, Bayesian optimal sensor placement for crack identification in structures using strain measurements, *Structural Control and Health Monitoring*. 25 (2018) e2137. <https://doi.org/10.1002/stc.2137>.
- [25] A. Lye, A. Cicirello, E. Patelli, An efficient and robust sampler for Bayesian inference: Transitional Ensemble Markov Chain Monte Carlo, *Mechanical Systems and Signal Processing*. 167 (2022) 108471. <https://doi.org/10.1016/J.YMSSP.2021.108471>.
- [26] M.C. Kennedy, A. O'Hagan, Bayesian calibration of computer models, *Journal of the Royal Statistical Society. Series B: Statistical Methodology*. 63 (2001) 425–464. <https://doi.org/10.1111/1467-9868.00294>.
- [27] J.L. Beck, S.-K. Au, Bayesian Updating of Structural Models and Reliability using Markov Chain Monte Carlo Simulation, (n.d.). <https://doi.org/10.1061/ASCE0733-93992002128:4380>.

- [28] H.-F. Lam, J.-H. Yang, S.-K. Au, Markov chain Monte Carlo-based Bayesian method for structural model updating and damage detection, *Structural Control and Health Monitoring*. 25 (2018) e2140. <https://doi.org/10.1002/stc.2140>.
- [29] J. Ching, Y.-C. Chen, Transitional Markov chain Monte Carlo method for Bayesian model updating, model class selection, and model averaging., *Journal of Engineering Mechanics*. 133 (2007) 816. [https://doi.org/10.1061/\(ASCE\)0733-9399\(2007\)133:7\(816\)](https://doi.org/10.1061/(ASCE)0733-9399(2007)133:7(816)).
- [30] C. Bishop, *Pattern Recognition and Machine Learning*, Springer, 2006.
- [31] S. Kullback, R.A. Leibler, On Information and Sufficiency, *The Annals of Mathematical Statistics*. 22 (1951) 79–86. <https://doi.org/10.1214/aoms/1177729694>.
- [32] M.P. Wand, J.T. Ormerod, S.A. Padoan, R. Frühwirth, Mean field variational bayes for elaborate distributions, *Bayesian Analysis*. 6 (2011) 847–900. <https://doi.org/10.1214/11-BA631>.
- [33] G. Consonni, J.M. Marin, Mean-field variational approximate Bayesian inference for latent variable models, *Computational Statistics and Data Analysis*. 52 (2007) 790–798. <https://doi.org/10.1016/j.csda.2006.10.028>.
- [34] R. Ranganath, S. Gerrish, D.M. Blei, Black Box Variational Inference, *Journal of Machine Learning Research*. 33 (2013) 814–822. <http://arxiv.org/abs/1401.0118> (accessed May 20, 2021).
- [35] A.C. Miller, N. Foti, R.P. Adams, Variational Boosting: Iteratively Refining Posterior Approximations, 34th International Conference on Machine Learning, ICML 2017. 5 (2016) 3732–3747. <http://arxiv.org/abs/1611.06585> (accessed May 16, 2021).
- [36] R.M. Neal, Slice sampling, *Annals of Statistics*. 31 (2003) 705–741. <https://doi.org/10.1214/aos/1056562461>.
- [37] M.D. McKay, R.J. Beckman, W.J. Conover, A Comparison of Three Methods for Selecting Values of Input Variables in the Analysis of Output from a Computer Code, *Technometrics*. 21 (1979) 239. <https://doi.org/10.2307/1268522>.
- [38] S. Mandt, J. McInerney, F. Abrol, R. Ranganath, D. Blei, Variational Tempering, *Proceedings of the 19th International Conference on Artificial Intelligence and Statistics, AISTATS 2016*. (2014) 704–712. <https://arxiv.org/abs/1411.1810v4> (accessed November 29, 2021).

- [39] H. Fu, C. Li, X. Liu, J. Gao, A. Celikyilmaz, L. Carin, Cyclical Annealing Schedule: A Simple Approach to Mitigating KL Vanishing, NAACL HLT 2019 - 2019 Conference of the North American Chapter of the Association for Computational Linguistics: Human Language Technologies - Proceedings of the Conference. 1 (2019) 240–250. <https://arxiv.org/abs/1903.10145v3> (accessed November 29, 2021).
- [40] R. Zhang, C. Li, J. Zhang, C. Chen, A.G. Wilson, Cyclical Stochastic Gradient MCMC for Bayesian Deep Learning, (2019). <https://arxiv.org/abs/1902.03932v2> (accessed November 30, 2021).
- [41] G. Huang, Y. Li, G. Pleiss, Z. Liu, J.E. Hopcroft, K.Q. Weinberger, Snapshot Ensembles: Train 1, get M for free, 5th International Conference on Learning Representations, ICLR 2017 - Conference Track Proceedings. (2017). <https://arxiv.org/abs/1704.00109v1> (accessed November 30, 2021).
- [42] I. Loshchilov, F. Hutter, SGDR: Stochastic Gradient Descent with Warm Restarts, 5th International Conference on Learning Representations, ICLR 2017 - Conference Track Proceedings. (2016). <https://arxiv.org/abs/1608.03983v5> (accessed November 30, 2021).
- [43] R.B. Gramacy, H.K.H. Lee, Cases for the nugget in modeling computer experiments, Statistics and Computing. 22 (2012) 713–722. <https://doi.org/10.1007/s11222-010-9224-x>.
- [44] C.E. Rasmussen, Z. Ghahramani, Bayesian Monte Carlo, n.d. <http://www.gatsby.ucl.ac.uk> (accessed May 15, 2021).
- [45] D.P. Kingma, M. Welling, Auto-encoding variational bayes, in: 2nd International Conference on Learning Representations, ICLR 2014 - Conference Track Proceedings, International Conference on Learning Representations, ICLR, 2014. <https://arxiv.org/abs/1312.6114v10> (accessed May 16, 2021).
- [46] D.P. Kingma, J.L. Ba, Adam: A method for stochastic optimization, in: 3rd International Conference on Learning Representations, ICLR 2015 - Conference Track Proceedings, International Conference on Learning Representations, ICLR, 2015. <https://arxiv.org/abs/1412.6980v9> (accessed May 16, 2021).
- [47] D.P. Kingma, J.L. Ba, Adam: A Method for Stochastic Optimization, 3rd International Conference on Learning Representations, ICLR 2015 - Conference

- Track Proceedings. (2014). <https://arxiv.org/abs/1412.6980v9> (accessed December 7, 2021).
- [48] MATLAB, (2020).
- [49] C. Safta, M. Khalil, H.N. Najm, Transitional Markov Chain Monte Carlo Sampler in UQtk, (2020). <https://doi.org/10.2172/1606084>.
- [50] M. Kitahara, S. Bi, M. Broggi, M. Beer, Nonparametric Bayesian stochastic model updating with hybrid uncertainties, Mechanical Systems and Signal Processing. 163 (2022) 108195. <https://doi.org/10.1016/J.YMSSP.2021.108195>.